THE IMPACT OF DIFFUSION ON BIOCHEMICAL ASSAY KINETICS IN 3D-HYDROGEL MICROARRAYS

JOSHA

josha.org

Journal of Science, Humanities and Arts

JOSHA is a service that helps scholars, researchers, and students discover, use, and build upon a wide range of content

Master Thesis

THE IMPACT OF DIFFUSION ON BIOCHEMICAL ASSAY KINETICS IN 3D-HYDROGEL MICROARRAYS
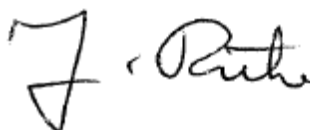
Mostafa Mahmoud

This thesis is submitted in partial fulfillment of the requirements of the University of Buenos Aires for the Master of Science degree in biomedical sciences, class of 2014.

The thesis was accomplished at the Laboratory of Chemistry and Physics of Interfaces (Prof. Dr. Jürgen Rühe) in the group of bioanalytical surfaces (Dr. Thomas Brandstetter)
Department of Microsystems Technology IMTEK
University of Freiburg
Freiburg im Breisgau, Germany

Author: Mostafa Mohamed Safwat Ahmed Mahmoud

Supervisor: Prof. Dr. J. Rühe, Laboratory of Chemistry and Physics of Interfaces, Department of Microsystems Technology IMTEK, University of Freiburg, Germany.

Co-supervisor: Prof. Dr. M. Mollerach, Professor of Microbiology, Department of Microbiology, Immunology and Biotechnology, School of Pharmacy and Biochemistry, University of Buenos Aires, Argentina.

Declaration

I hereby confirm that this master thesis at hand is solely my own written work and that no other sources, than those indicated in the references, were used.

All text passages and diagrams, quoted or paraphrased, from these sources have been properly acknowledged as such and fully cited.
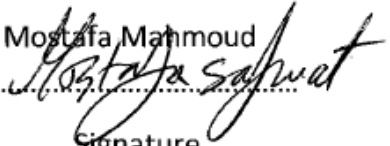
This thesis has not been submitted in the same, similar or even partial version to another examination board and was not published elsewhere.

Freiburg, November 1, 2014

………………………………………

Place, Date

Mostafa Mahmoud

………………………………………

Signature

ABSTRACT

Microarrays are powerful and versatile analytical tools. They can address the complex diagnosis of various diseases and disorders in a fast, reliable and simple manner. They consist of very small test sites in form of spots on which various biochemical assays can be performed simultaneously. In the past few years, this technology has developed a lot with the implementation of novel surface chemistries, detection techniques, and different assay formats. 3D-hydrogel microarrays were developed using unique immobilization techniques based on hydrophilic polymer networks. The 3D polymer network attaches and immobilizes the capture molecules onto the surface in form of a spot with molecules immobilized both on the surface and inside the gel matrix. This retains the molecule's natural confirmation and structure and enables higher immobilization efficiency, which allows for higher sensitivity. However, the achieved sensitivities are still far from the theoretical limit and in many cases, long incubation times are required. These limitations are caused by both the resolution of the used detection techniques and the assay kinetics. This hinders the transfer of the technology from the laboratory to routine diagnostics.

The kinetics of a biochemical assay in a microarray can be controlled either by the transport of molecules to the spot or by the binding interaction itself. This work focuses on studying the assay kinetics in 3D-hydrogel microarrays in order to understand and characterize the limiting step for signal development. To simulate conditions of high affinity binding partners and therefore reduce the influence of the reaction kinetics, the biotin-streptavidin system was selected as the biological model for this work.

A microarray to study the kinetic processes involved in the signal development was designed and the optimum working concentrations for kinetic characterization were defined. To confirm the mass transport limited kinetics, the measured kinetics was compared to the ideal reaction kinetics depending on the affinity parameters for biotin-streptavidin interaction. The ideal reaction kinetics was three orders of magnitude faster than measured kinetics. The two-compartment model, which is widely used to describe the assay kinetics in 2D microarrays, was used to fit the observed kinetics. However, a deviation from the model after the initial phase of signal development was observed. A hypothesis was made that this deviation is due to an additional diffusion step in the hydrogel. Therefore, a microarray model to study this diffusion step was designed. In this model, the microarrays were dip coated with hydrogel layers of various thickness and mesh sizes. This model simulated conditions where the signal development should depend only on the diffusion through the hydrogel. The observed signal development was linear and one order of magnitude slower than for non-coated microarrays. The slope corresponded to the mass transport rate through the hydrogel. This behavior was comparable to the observed deviations from the two-compartment model in the later phases of the measured kinetics of non-coated microarrays. Therefore, to account for this slow signal development due to diffusion in the hydrogel, the model was modified by including an additional exponential term. The modified

model showed very good agreement with the overall measured kinetics (r^2=0.992 and x^2=0.06).

The developed model can be used in the future to describe the assay kinetics in 3D-hydrogel microarrays and this will allow for the better understanding of the imposed limitations. Moreover, it will facilitate the selection of the design parameters such as time of incubation, spotting concentrations, hydrogel concentration and the application of mixing to realize systems that provide high sensitivities in short incubation times.

RESUMEN

Las micromatrices o microarreglos ("microarrays") son herramientas de análisis poderosas y versátiles. Pueden resolver el complejo diagnóstico de varias enfermedades y desórdenes en forma rápida, confiable y simple. Este formato experimental consiste en pequeños sitios de ensayo en forma de puntos en donde varias determinaciones bioquímicas se pueden realizar simultáneamente. En los últimos años, esta tecnología se ha desarrollado mucho con la implementación de la nueva química de superficie, nuevas técnicas de detección, y diferentes formatos de ensayos. Los microarreglos en hidrogeles tridimensionales (3D-hidrogeles) fueron desarrollados usando técnicas de inmovilización únicas basadas en redes poliméricas hidrofílicas. La red polímera 3D inmoviliza las moléculas capturadas en la superficie en forma de un punto con moléculas inmovilizadas en la superficie y dentro del gel matriz. Éste retiene las conformaciones naturales de las moléculas y su estructura, posibilitando una eficiencia mayor en la inmovilización, que permite mayor sensibilidad. De todos modos, la sensibilidad alcanzada está todavía lejos del límite teórico y en muchos casos, se requieren largos períodos de incubación. Estas limitaciones son causadas tanto por la resolución de las técnicas de detección utilizadas como por la cinética de los ensayos. Esto dificulta la transferencia de esta tecnología del laboratorio al diagnóstico de rutina.

La cinética de un ensayo bioquímico en un microarreglo se puede controlar, ya sea por el transporte de moléculas hacia el punto o por la propia interacción de unión. Este trabajo se centra en el estudio de la cinética de ensayo en micromatrices de hidrogeles-3D, para comprender y caracterizar el paso limitante para el desarrollo de señal. Para simular las condiciones de asociación de alta afinidad de y por lo tanto reducir la influencia de la reacción cinética, el sistema biotina-estreptavidina fue seleccionado como el modelo biológico para este trabajo.

Para estudiar los procesos cinéticos implicados en el desarrollo de señal de diseño una micromariz y se definieron las concentraciones óptimas de trabajo para la caracterización cinética. Para confirmar la cinética limitada del transporte de masa, se comparó la cinética medida con la reacción cinética ideal, de acuerdo a los parámetros de afinidad para la interacción biotina-estreptavidina. La reacción cinética ideal fue tres órdenes de magnitud más rápida que la cinética medida. El modelo de dos compartimentos, que es ampliamente utilizado para describir la cinética de ensayo en microarreglos 2D, se utilizó para ajustar la cinética observada. Sin embargo, se observó una desviación del modelo después de la fase inicial de desarrollo de señal. Se generó una hipótesis sobre que ésta desviación se debe a un paso de difusión adicional en el hidrogel. Por lo tanto se diseñó un modelo de microarreglo para estudiar esta etapa de difusión. En este modelo, las micromatrices fueron recubiertas en profundidad con varios espesores y tamaños de malla de hidrogel. Este modelo simuló condiciones donde el desarrollo de señal debería depender sólo de la difusión a través del hidrogel. El desarrollo de señal observada fue lineal y un orden de magnitud menor que para microarreglos no recubiertos. La pendiente correspondió a la tasa de transporte de masa a través del hydrogel. Este comportamiento fue comparable a las desviaciones observadas a

partir del modelo de dos compartimentos en las fases posteriores a la cinética medida en microarreglos no recubiertos. Por lo tanto, para dar cuenta de este desarrollo de señal lento debido a la difusión en el hidrogel, los modelos fueron modificados mediante la inclusión de un término exponencial adicional. El modelo modificado mostró muy buen acuerdo con la cinética medida general($r2 = 0,992$ y $x2 = 0,06$).

El modelo desarrollado puede ser utilizado en el futuro para describir la cinética de ensayo micromatrices de hidrogel 3D permitiendo la mejor comprensión de las limitaciones impuestas. Además, facilitará la selección de los parámetros de diseño tales como el tiempo de incubación, concentraciones de puntos, la concentración de hidrogel y la aplicación de la mezcla para realizar sistemas que proporcionan altas sensibilidades en tiempos de incubación cortos.

CONTENTS

CONTENTS

ABBREVIATIONS

ATR	attenuated total reflection
CC	coupling control
CCD	charge coupled device
Cy5	Cyanine 5 fluorescent dye (excitation wavelength ≈ 646nm)
DI water	deionized water
DMAA	dimethylacrylamide
DOL	degree of labeling (number of fluorophores per biomolecule)
ELISA	enzyme linked immuno sorbent assay
MABP	4-methacryloyl-oxy-benzophenone
NaPi	sodium-phosphate buffer
NC	negative control; spot without biological species
NHS-ester	N-hydroxy succinimide ester
PBS	phosphate buffered saline
PBST	PBS (1x) with 0.1 v/v Tween 20
PDMAA	polydimethylacrylamide
SELEX	Systemic evolution of ligands by exponential enrichment
SEM	Standard error of the mean
Tween	Tween 20 (polyoxyethylen(20)-sorbitan-monolaurate)

Table of figures

1. INTRODUCTION

1.1. IN-VITRO DIAGNOSTICS: IMMUNOASSAYS

In-vitro diagnostic (IVD) tests are biochemical assays performed extracorporeal that are capable of quantifying biomolecules in biological samples and fluids. They evaluate both the normal and altered human physiological functions. Combined with physical examination and in-vivo diagnostics (e.g. Nuclear magnetic resonance imaging and computed tomography), they provide valuable information for treatment decisions. Immunoassays are the most commonly performed IVD format for protein measurements (Vitzthum et al., 2005).

Immunoassays are very important routine diagnostics tools in today's laboratory practice. An immunoassay is a biochemical test that detects or measures the concentration of a biomolecule through the use of an antibody. They depend on the high affinity of antigen-antibody biomolecular interactions following the lock and key theory introduced by Emil Fischer, 1894. (Hennion and Barcelo, 1998; Killard et al., 1995).

Antibodies or immunoglobulins (Ig) are Y shaped proteins produced by the B-lymphocytes of the adaptive immune system. They consist of paired heavy (50-70 KDa) and light (25 KDa) polypeptide chains. Antibodies can be divided into five different subclasses depending on the isoform of the constant region of their heavy chains (IgM, IgD, IgG, IgA and IgE). The most abundant immunoglobulin isoform found in plasma is the immunoglobulin G (IgG) (Figure 1.1). IgG molecule consist of two heavy and two light chains linked by a disulfide bond. The chains consist of similar yet not identical amino acid sequences of about 110 residues long known as the immunoglobulin protein domain. The light chain consists of two immunoglobulin domains (about 220 amino acid residues) while the heavy chain consists of four immunoglobulin domains. The variability in both the heavy and light chain is limited to the first immunoglobulin domain and the remaining domains are constant between immunoglobulins from same isoform. This variable part of the chains defines the antibody ability to bind to specific antigen (Janeway, 2005).
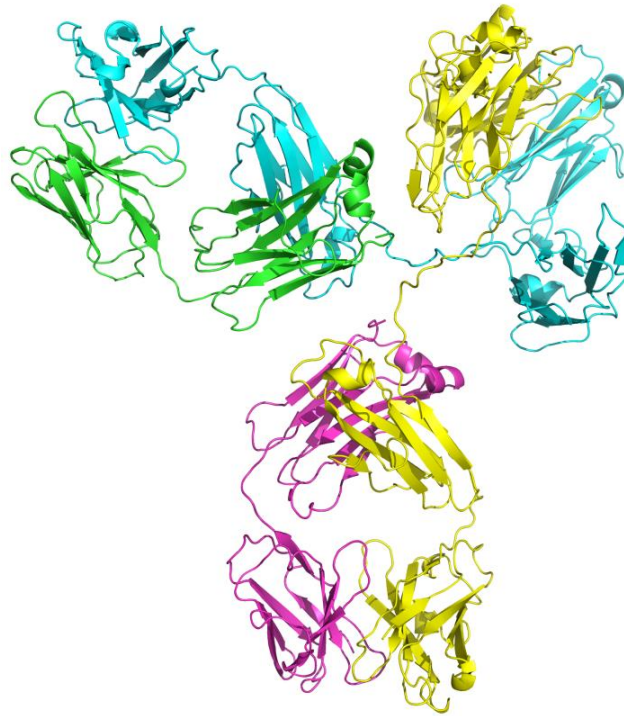
Figure 1.1 Crystallographic structure of an intact IgG1 monoclonal antibody. Image generated by PyMOL (Schrodinger, 2010) using the RCSB PDB (www.rcsb.org) entry ID 1IGY (Harris et al., 1998).

1.1.1. TYPES OF IMMUNOASSAYS

Immunoassays can be performed in different formats (Rubina et al., 2005) such as:

Direct immunoassay:

In this assay type, the analyte is labeled and bound to an antibody, which is immobilized on the substrate (Figure 1.2.a).

Indirect immunoassay:

The antigen to be quantified is immobilized on the solid substrate and the sample containing the antibody is used for the assay (Figure 1.2.b). As an example, indirect immunoassay is commonly used for the diagnosis of HIV. In this assays the viral antigens are immobilized on solid substrate and patient's serum containing anti-HIV antibodies is incubated to detect the disease (Iweala, 2004).

Sandwich immunoassay:

In a sandwich immunoassay, the antigen to be measured should at least have two different epitopes for the binding of antibodies (Self and Cook, 1996). One antibody is immobilized on the substrate called capture antibody and another labeled antibody is used for the detection namely, the detection antibody (Figure 1.2.c) (Rubina et al., 2005). First, the analyte is added to the capture antibody followed by a washing step to remove non-bound molecules. Then

the detection antibody is added in excess, and after another washing step the signal can be measured and quantified (Marco et al., 1995).

Non-competitive immunoassay:

The antigen binds to the free antibody binding sites with no other competing species present in the sample. This assay could be either direct, indirect or sandwich format (Hennion and Barcelo, 1998).

Competitive immunoassay:

This assay type depends on the phenomenon of competition between labeled and unlabeled analyte molecules for a limited number of binding sites (Figure 1.2.d). There are two methods to measure the signal in this assay. a) Washing out the unbound labeled analytes and then measuring the signal of either the bound or the unbound analytes or b) saturating the binding sites with a known concentration of labeled analyte and measuring the decrease of signal. In both cases the decrease of binding of labeled analyte is proportional to the concentration of unlabeled sample (Marco et al., 1995).
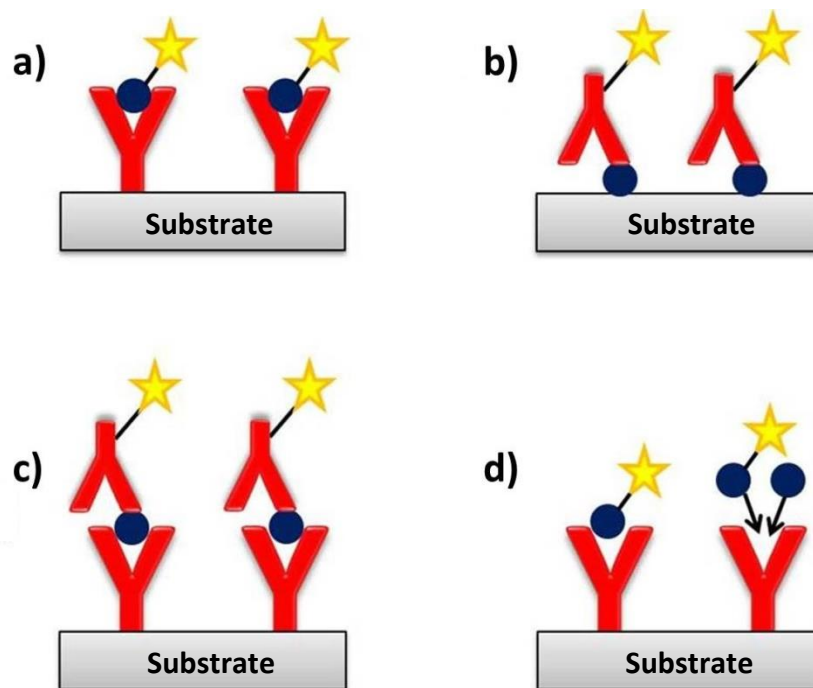
Figure 1.2 Schematic representation of different immunoassays. The red (Y) represents the capture antibody, the blue circle is unlabeled analyte, and the star symbol designates a labeled species. (a) Direct immunoassay where directly labeled analyte bind to capture antibody, (b) indirect immunoassay where labeled antibodies bind to the immobilized analyte, (c) non-competitive sandwich immunoassay with both unlabeled analyte and labeled detection antibodies, and (d) direct competitive immunoassay where both labeled and unlabeled antigen compete for limited binding sites.

Enzyme-Linked Immunosorbent Assay (ELISA):

In 1971, Van Weemen et al. introduced for the detection and quantification of antigens the Enzyme Linked Immunosorbent Assay (ELISA). Since then ELISA has become a standard test in routine diagnostics. ELISA is a heterogeneous immunoassay where antibodies are immobilized on the surface. ELISA uses a special detection strategy based on an enzyme label. The sample and a known amount of enzymatically labeled antigen are then added to the well and incubated at room temperature for a period of 10-60 minutes. They compete for the limited number of binding sites according to the law of mass action (Hennion and Barcelo, 1998). Increasing the concentration of the analyte in the sample will lead to a displacement of enzymatically labeled antigen from the limited binding sites. After incubation, there is a washing step to separate bound species from unbound ones. The enzyme labeled antigen is quantified by adding a substrate specific to the enzyme. The enzyme catalyzes the conversion of the substrate to a colored product. The color intensity is proportional to the amount of enzyme conjugates and inversely proportional to the analyte concentration in the sample. The color can be readout using standard spectrophotometers (Figure 1.3). Using standard samples with known concentrations allow for the quantitative evaluation of the sample (Hennion and Barcelo, 1998).
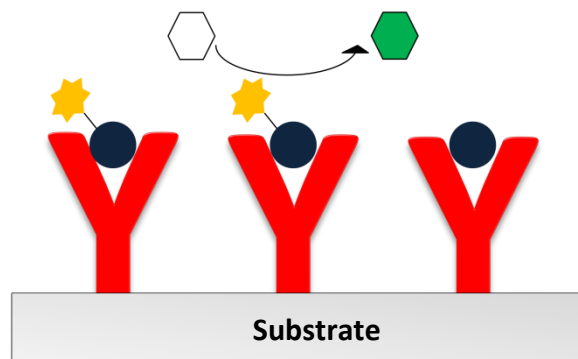
Figure 1.3 Schematic showing the direct competitive ELISA principle, where the antibodies (red (Y) symbol) are immobilized on a solid substrate and an enzyme labeled antigen (blue circle with orange star) is added to compete with the antigen in the sample (blue circle). After incubation and washing steps, an enzyme substrate (white pentagon) is added which is converted by the enzyme to a colored product (green pentagon).

1.2.   MICROARRAYS

Most diagnostic immunoassays are performed in centralized laboratories, relying on sophisticated analytical methods requiring expensive bulky equipment, large amounts of sample, highly trained personnel and special requirements for GLP (Yager et al., 2006). This makes it a time and resources consuming process. These settings are not desirable in many cases, e.g. when there is a need for fast analysis especially for the diagnosis of patients in intensive care unit (ICU) or the patients have only a limited mobility. The need for fast results and for a reduction of the sample size as well as the growing importance of proteomics was the motive behind developing the first protein microarray in 1989 (Ekins et al., 1989). Microarrays are a collection of individual assays in the form of spots on a solid substrate (Figure 1.4). Each spot resembles a well of the microtiter plate typically used for ELISA. This miniaturization allows for the fast and parallel multiplex detection of various analytes and offer advantages over traditional immunoassays (Berrade et al., 2011; Angenendt, 2005; Zhu and Snyder, 2003).

1. It theoretically increases the sensitivity leading to lower limits of detection.
2. It saves both the sample and the antibodies through using less amounts and volumes of reagents per assay.
3. Faster assay speeds and higher throughput.

In 1989 Ekins (Ekins et al., 1989) described this unique immunoassay system in the ambient analyte theory. Based on law of mass action, it states that this system unlike conventional ones is capable of evaluating the analyte concentrations in a sample regardless of the sample volume. When very small amounts of antibodies are introduced to the sample, the analyte molecules are depleted due to the binding event. However, the proportional bound is small (less than 1% of the total) and can be ignored. This allows the detection and quantitation of very low analyte concentrations in the range of 10^{-19}-10^{-16} M (Kusnezow et al., 2006a).
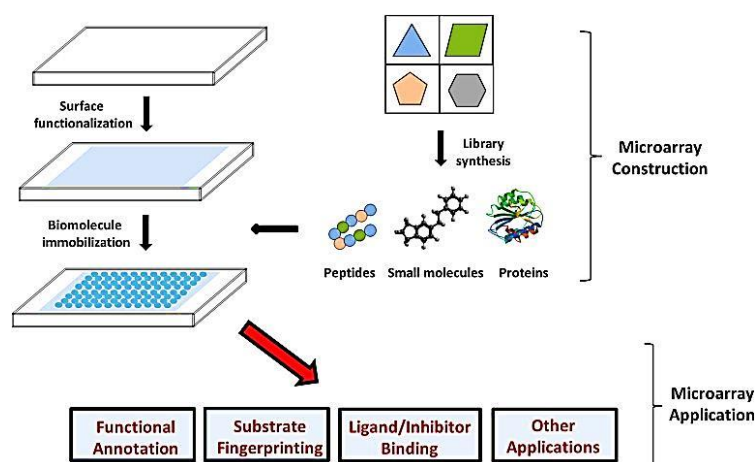
Figure 1.4 Schematic representation of a microarray construction and application (Sun et al., 2013).

1.2.1. PRINTING OF MICROARRAYS

1.2.1.1. CONTACT PRINTING

Contact pin printing use a robotic setup with solid, split, or quill pins to transfer the protein containing solution from a reservoir and deposit it onto the surface of the solid microarray substrate (Figure 1.5). The pin acquires a specific volume of the print solution through dipping it into the reservoir and withdrawing it at a certain speed. The amount of liquid depends on the tip geometry, the surface chemical composition of the tip and the withdrawal speed. The pin is then moved to the appropriate location on the chip and then a light contact between the pins and the surface results in the deposition of typically nano liters of the protein liquid onto the chip surface. The morphology and size of the resulting spot depends on the drop volume, the concentration of the protein and other non-volatile compound, on the surface tension of the droplet, the drying conditions and the surface properties of the chip (Romanov et al., 2014). These printers are easy to use and very flexible concerning the properties of the print solution (different viscosities or the presence of charges). However, they suffer from the following drawbacks (Romanov et al., 2014):

1. Low reproducibility of the deposited drop volume.
2. Time consuming and tedious process.
3. Proteins can adsorb to the solid surface of the pins.
4. Possible Cross contamination of different print solutions if different solutions are printed with one pin and the pin is not washed properly.
5. The pins can damage the substrate surface.
6. Potential Clogging of the pins (especially for split and quill pin) and inability to print viscous solutions with high precision.
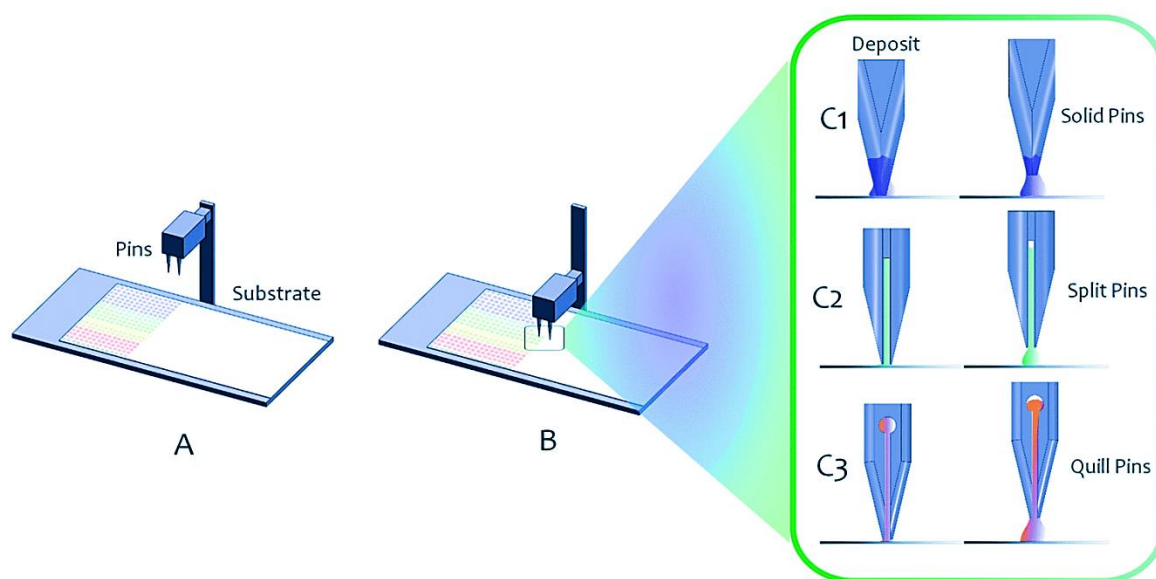
Figure 1.5 Schematic representation of contact pin printing. (A) The robot assembly with the substrate and the pins loaded in the print head then in (B) it touches the surface to deposit the solution as a spot. The various types of pins are shown (C1) solid pin, (C2) split pin, and (C3) quill pin containing a reservoir (Romanov et al., 2014).

1.2.1.2. NON-CONTACT PRINTING

The drawbacks of the contact printing methods were the motive behind the development of non-contact printing. Non-contact printers adopted some key features of the technology from inkjet printing technology and adapted it to the printing of solutions containing biomolecules. The printer consists of ink cartridges containing the protein solution and a print head nozzle. The printer ejects the solution onto the surface without contact using one of three ejection mechanisms: 1.) thermal inkjet 2.) valve-jet, or 3.) piezo actuation. In thermal inkjet, a rapid volume exchange of a gas bubble leads to ejecting the liquid. This is attained through heating the gas rapidly in the ink chamber (Figure 1.6.A). Valve-jet printers operate in contrast to this with a continuous high pressure in the ink reservoir and the solution ejection is controlled through a valve that can be opened to eject the drops of liquid (Figure 1.6.B). In piezo actuation, the solution to be printed is ejected as drops by the force exerted by the piezo crystal on the print nozzle (Figure 1.6.C) (Romanov et al., 2014). The main advantages of this technology as reviewed by Romanov and coworkers (Romanov et al., 2014) are:

1. Non-contact printers can print on any surface without touching it, so that the danger of surface damage can be greatly reduced.
2. As fewer parameters are involved, the process allows potentially better spot reproducibility
3. As no mechanical movements are involved such as moving the pin up and down in contact printing a faster throughput can be achieved. The ejection of droplets with kilohertz frequencies is possible.
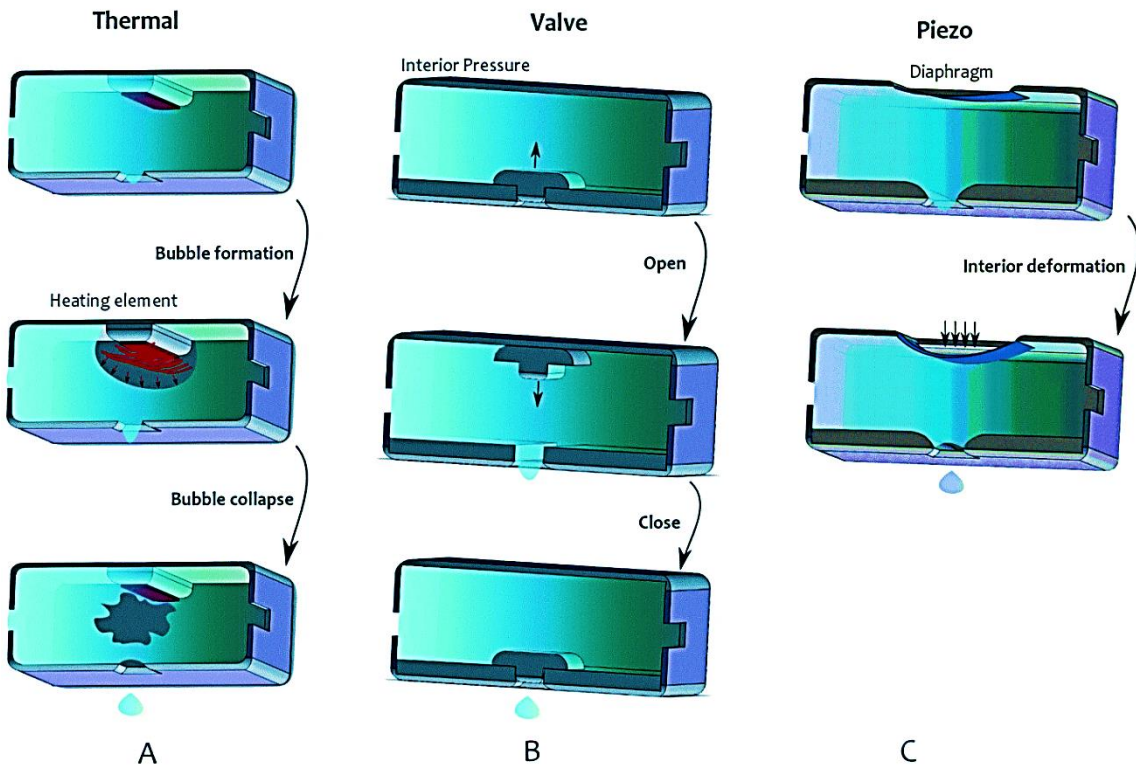
Figure 1.6 Schematic showing the different non-contact printers (Romanov et al., 2014). (A) Thermal inkjet, heating creates a bubble within the reservoir and leads to liquid ejection upon bubble collapse, (B) valve-jet where the liquid ejection is controlled by the opening and closing of a valve, and (C) piezo actuation where a piezo crystal exerts force on the diaphragm leading to liquid ejection.

1.2.2. IMMOBILIZATION OF PROTEINS ON MICROARRAYS

Protein Microarrays are prepared by spotting the proteins on a planar or micro-structured solid surface using a contact or contactless microarray printer. Immobilization means attaching the protein molecules to the surface of the solid substrate resulting in partial or complete loss of mobility. Different immobilization techniques are used utilizing different chemical and physical properties. The molecules should be immobilized using a suitable technique to preserve their natural conformation and function. The choice of the suitable strategy depends on the physicochemical and chemical properties of both the molecule and the surface (Rusmini et al., 2007).

1.2.2.1. 2D-IMMOBILIZATION APPROACHES (2D MICROARRAYS)

Conventionally biological species such as proteins are immobilized on a planar activated surface in a 2D approach. Usually, the chemical strategy chosen to attach a biomolecule to the surface highly affects the properties of the resulting protein biochip (Jonkheijm et al., 2008).

The 2D-immobilization strategies can be further divided into 3 different categories. Physical, bio-affinity and covalent immobilization techniques (Rusmini et al., 2007).

Physical immobilization is achieved through the adsorption of proteins on surfaces via ionic, hydrophobic and polar interactions. The proteins adsorb to the surface in random orientations to minimize the repulsions with both the surface and other adsorbed proteins. Drawbacks of this strategy are the weak attachment and the random orientation. Proteins active sites are blocked by steric hindrance and the proteins detaches during washing steps in an immunoassay (Rusmini et al., 2007).

Bio-affinity immobilization: It relies on the non-covalent biochemical affinity interaction of biomolecules such as the biotin-avidin system. This system is one of the strongest biomolecular interaction described ($K_d = 10^{-15}$ M^{-1}) (Diamandis and Christopoulos, 1991). The bond formation is fast and is not affected by conditions such as pH, temperature, solvents and denaturing agents. The surface must be functionalized by either avidin or biotin through direct immobilization through either adsorption or covalent attachment. A typical multilayer of biotin-avidin-biotin is achieved through functionalizing the surface with biotin and then binding the avidin molecules, which act as a binding bridge for biotinylated biomolecules. Biomolecules can be conjugated to biotin without altering their conformation, size or functionality. However, the most common biotinylation reaction depends on the NHS-ester of the biotin to target amine groups in proteins (Rusmini et al., 2007).

Covalent Immobilization: Proteins can be covalently bound to a functionalized surface. This attachment is either nonspecific or site-specific. Nonspecific covalent attachment relies on the abundant and accessible functional residues on the surface of the protein. They serve as anchoring points for the protein on the surface. A simple approach is to immobilize the biomolecules through a free radical crosslinking of the photo-reactive groups (thymine) of the molecule itself to a polymer film on the surface by UV-irradiation forming self-assembled monolayers (Freidank, 2005). Another approach where the surfaces are first functionalized with N-hydroxysuccinimide (NHS) and then reacted with the amine groups present in lysine residues on protein surface. This forms stable amide ester bonds (Figure 1.7.a). As an alternative the surface could be activated with an aldehyde group that reacts with the amine groups forming a secondary amine link (Figure 1.7.b). Other nonspecific covalent immobilization techniques make use of the different groups present and accessible on a protein surface such as thiol (melamide bonds), carboxyl (through carboiimide activation) and hydroxyl (epoxy chemistry) groups. Drawbacks of nonspecific covalent reactions are denaturation of the proteins, loss of flexibility, heterogeneity of the attachment and loss of function.

On the other hand, site-specific covalent immobilization requires the functionalization of the molecules and the activation of the surface. This ensures the orientation and the uniform attachment of proteins to the surface. The covalent reaction depends on the coupled functional group to the protein and the activation of the surface. Proteins functionalized with azide or alkyne groups for example can react with a surface activated with the opposite group through 1, 3 dipolar cycloaddition reaction also known as click chemistry (Figure 1.8).
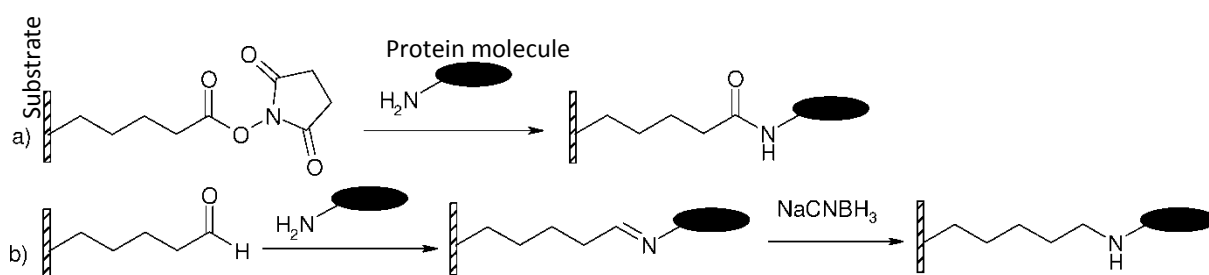
Figure 1.7 Schematic representation of nonspecific covalent immobilization strategies depending on a) NHS activated surface and b) aldehyde activated surface (Rusmini et al., 2007).
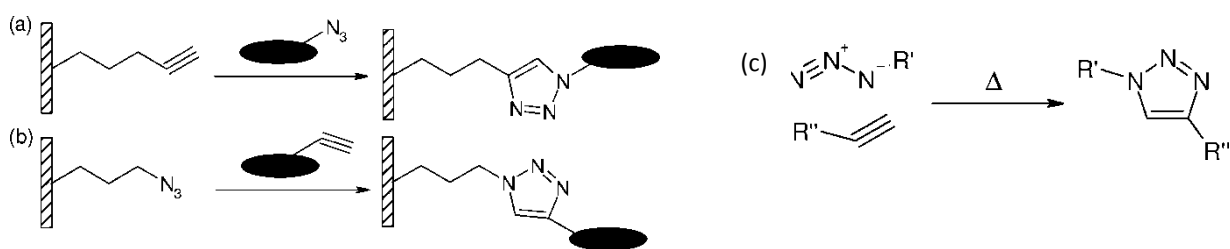
Figure 1.8 Schematic representation of site-specific covalent immobilization strategy depending on a) azide functionalized protein on alkyne modified surface, b) Alkyne functionalized protein on azide functionalized surface and c) scheme of 1, 3 cycloaddition reaction (Rusmini et al., 2007).

1.2.2.2. 3D-HYDROGEL IMMOBILIZATION STRATEGY

Two dimensional immobilization techniques have a strongly limited protein binding capacity due to the limited area of the surface (Moschallski, 2007).

To overcome this limitation and to increase the surface density of immobilized biomolecules, different methods based on polymer hydrogels as a new immobilization strategy were described (Rendl et al., 2011; Moschallski et al., 2010; Zubtsov et al., 2007; Rubina et al., 2003). A simple approach developed by Rendl et al. allows for fast production of microarrays. First, the biological probes are mixed with photoactive polymer in a buffer solution. The mixture is then spotted on unmodified plastic surfaces followed by a brief UV-irradiation to cross link the polymer. This process immobilizes the biomolecules within the polymer network and attaches them to the surface. This results in the functionalization of the surface in a spatially confined manner. The use of plastic substrates abolishes the need of complex substrates functionalized with reactive groups such as NHS or aldehydes (Rendl et al., 2011).

The immobilization technique developed by Rendl et al. was based on a poly dimethyl acrylamide (DMAA) copolymer containing the photoactive cross-linker 4-Methacryloyl-oxy-benzophenone (MABP) and Styrene-4-sulfonic acid sodium salt (SSNa) (Figure 1.9 A). Upon UV-irradiation, a photochemical reaction takes place causing the polymer network to cross-link, immobilize the biomolecules and attaches to the surface. The photo reactive MABP moiety undergoes n-π* or π-π* transition[1] forming a biradical triplet state. This state enables the molecule to abstract hydrogen atom from any neighboring aliphatic C-H group, then the two resulting carbon radicals are recombined to form C-C bond (Figure 1.9 B) (Rendl et al., 2011; Moschallski, 2007; Toomey et al., 2004).

---

[1] (n-π*) and (π-π*) are molecular electronic transitions where the excitation of an electron in the non-bonding (n) or the bi bonding (π) molecular orbitals causes its transition to the (π*) anti-bonding molecular orbital.
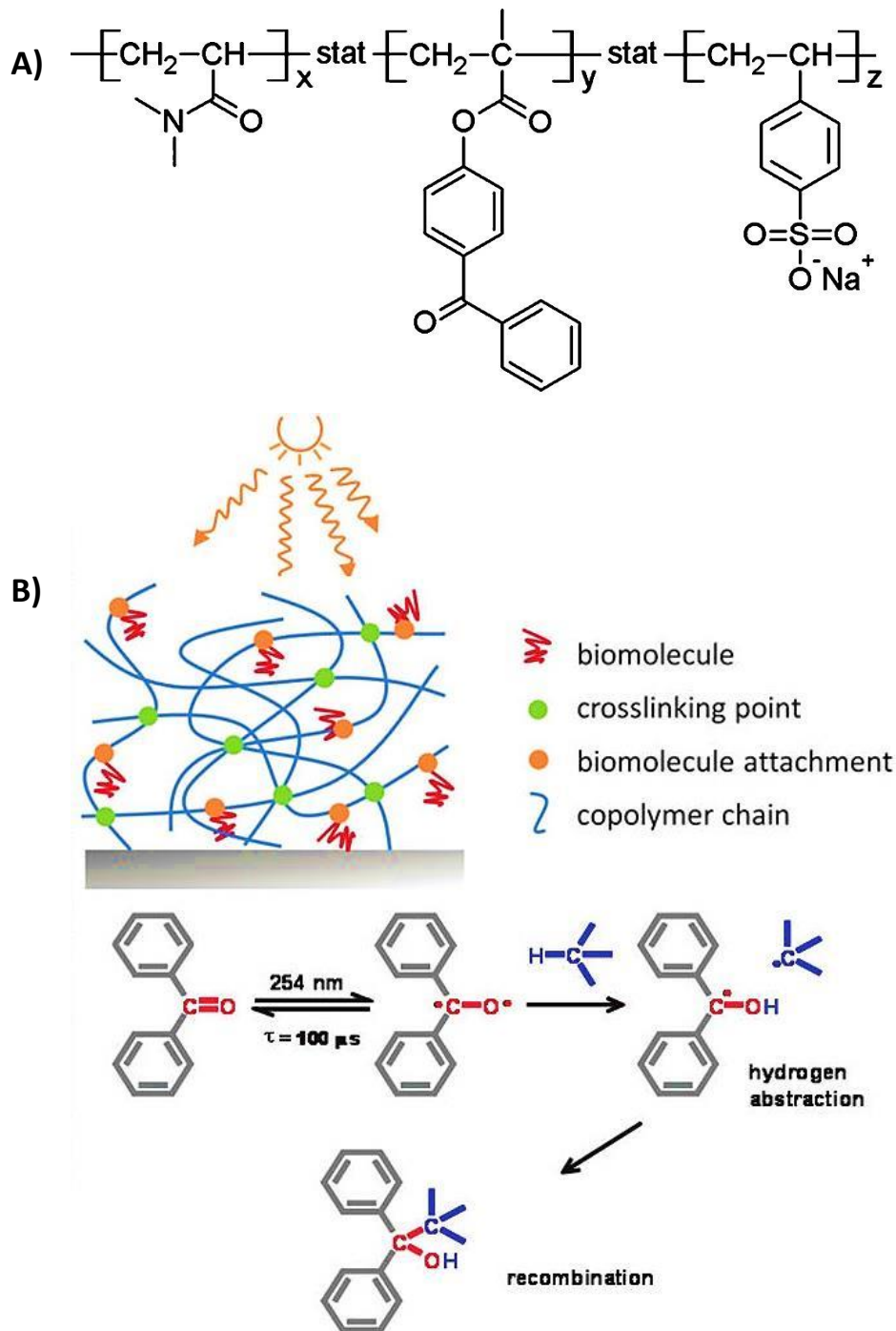
Figure 1.9 A) Chemical structure of the PDMMA-5%MABP-2.5%SSNA co-polymer used in the 3D immobilization and B) the crosslinking reaction of the benzophenone moiety. Upon UV-irradiation the MABP undergoes n-π* or π-π* forming a biradical triplet state. Then, a hydrogen abstraction from C-H from neighboring protein and then recombines forming C-C stable bond (Rendl et al., 2011).

1.2.3. DETECTION METHODS FOR PROTEIN-MICROARRAYS

1.2.3.1. LABEL BASED DETECTION TECHNIQUES

Immunoassay detection techniques depend mostly on the use of different labels, according to the assay format and purpose. Proteins can be labeled with a variety of different tags such as radioisotopes, fluorescent, chemiluminescent or affinity tags (Hall et al., 2007). However, fluorescent labels are usually preferred due to the high sensitivity, the – compared to radioisotope labeling, which could be also very sensitive – simple sample handling, as well as the availability of easy and fast labeling procedures. Fluorescent labels can be detected using standard fluorescence readers (Peoples and Karnes, 2008; Bally et al., 2006). Despite of all the advantages offered by the label based detection, it still faces some drawbacks. The main concerns are the loss of activity or conformation of the protein after the labeling procedures, steric hindrance, photobleaching and sensitivity of the light emission due to variations in the environment, such as pH changes (Hall et al., 2007; Bally et al., 2006; Bange et al., 2005).

Special setups have been designed to allow for a recording of the fluorescence intensity during the course of a reaction and thus time resolved measurements of the binding process. Based on the optical phenomenon of total internal reflection fluorescence (TIRF), Harrick (Harrick, 1960) developed a setup where only fluorescent molecules close to the surface can be measured. A light beam is coupled into the surface of the slide under a certain angle of incidence. The light is then totally reflected at the interface producing an evanescent field (Figure 1.10). The field's intensity decreases exponentially with increasing the distance from the surface allowing only the excitation molecules in close vicinity to the surface (Neumann, 2006; Lehr et al., 2003). A CCD camera detects the light emitted by the molecules after passing through a wavelength selective filter, which especially blocks out the exciting light. The ATR process allows the quantification of specific signals due to binding events on the surface and reduces the contribution of free molecules to the recorded signals.
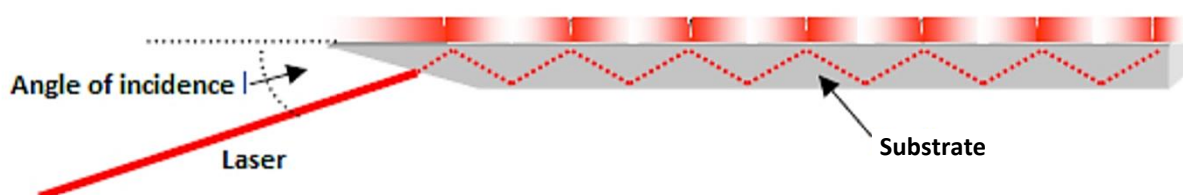
Figure 1.10 Schematic representation of the coupling of the laser in a TIRF setup (Neumann, 2006).

1.2.3.2. LABEL FREE DETECTION TECHNIQUES

Label free detection methods were developed in an approach to overcome the problems that label detection suffered from. According to Ramachandran and co-workers (Ramachandran et al., 2005) any label free method intended for detection of microarrays should fulfill a number of requirements such as

1. Ability to detect multiplex microarrays.
2. Ability to detect small molecule binding events.
3. High sensitivity and a wide dynamic range of detection.

Label free detection measures any changes induced by the biochemical interaction in the inherent properties of the molecules itself such as mass, dielectric or optical properties (Gonzalez-Gonzalez et al., 2012; Ray et al., 2010). Various label-free detection techniques based on the property measured were developed. These include surface plasmon resonance (SPR), ellipsometry, scanning kelvin nanoprobe and atomic force microscope (AFM) (Gonzalez-Gonzalez et al., 2012; Ray et al., 2010; Hall et al., 2007; Ramachandran et al., 2005).

1.2.4. SENSITIVITY OF MICROARRAYS

The detection of a given biomarker (analyte) on a microarray is governed by the sensitivity of the used detection technique and the number of molecules captured on the surface. Assuming the reaction proceeds for infinite times and the maximum amount of analyte molecules is bound on the surface. In this case, the limit of detection will be given by the ability of the device to detect this amount. This can be overcome using highly sensitive readout devices and/or signal amplification strategies. However, the time needed to capture sufficient amount of analyte molecules (i.e. higher than the device detection limit with or without amplification) will depend on the kinetics of the reaction. The binding kinetics of a biochemical reaction can be limited by the affinity of the capture molecule or the mass transport of the analyte in solution to bind to the capture molecule. The reaction rate will determine the time needed for binding detectable amounts of analyte molecules on the surface of the microarray. In ideal situations, the rate of the reaction will be controlled by the association and dissociation rate constants of the binding partners (i.e. the affinity of the system) (Kusnezow et al., 2006c). This limitation is addressed by the development of highly affine capture molecules.

For high affinity systems, therefore the rate-limiting step will be the mass transport of the analyte molecules. The diffusion/mass transport limited binding reaction can be described using the two-compartment model. This model divides the binding interaction into two separate steps a) the transport of analyte molecules in solution to reach the capture molecules, and b) the binding event itself.

1.3. STATE OF THE ART OF DIAGNOSTIC MICROARRAYS

In the past years, microarrays have developed greatly benefiting from the advances in the individual fields, which are involved in the manufacturing processes of microarrays. The most important developments made in those fields were discussed in the previous chapters. These individual technologies must be combined and optimized to detect and quantify biomarkers with high sensitivity in short incubation times.

In the field of diagnostic microarrays, the following reviews (Abel et al., 2014; Sun et al., 2013; Hall et al., 2007; Pavlickova et al., 2004; Glökler and Angenendt, 2003; Cahill, 2001) give an overview on proof-of-principle experiments for different possible applications using protein microarrays. Joos et. al (Joos et al., 2000) developed a serum profiling microarray for the diagnostic of autoimmune diseases. The developed microarray can analyze 18 known autoantigens simultaneously with high sensitivity (down to 40 fg) and specificity. As an example for the multiplexing capabilities of microarrays, Sreekumar et al. (Sreekumar et al., 2001) developed arrays for the profiling of cancer cells. The arrays contained 146 different antibodies. The developed microarrays were able to monitor alterations of protein levels in carcinoma cells treated with ionizing radiation.

Another recent example by Buchegger and co-workers (Buchegger and Preininger, 2014) report on the development of 4 sepsis diagnostic microarrays. The printing was done using a contact printer, probes were immobilized by covalent attachment to epoxy activated glass substrates, and fluorescence spectroscopy was used for detection. The authors studied different assay types and signal amplification methods to optimize the microarrays for the detection of different biomarkers for sepsis. The assays differed in their processing time according to the detection strategy. In the first assay Figure 1.11 (I), they used a biotin labeled antibody detected by fluorescently labeled streptavidin. The fastest assay was processed in 4 hours Figure 1.11 (II), and was based on a directly labeled detection antibody. To improve the sensitivity, the authors introduced two amplification strategies in the third and fourth array. The first was based on an enzymatic amplification and the second was achieved using a third antibody (carrying the same label as the detection antibody) to target the detection antibody Figure 1.11 (III) and (IV). The use of the complex detection techniques allowed reaching one order of magnitude lower limits of detection compared to the first two assays. However, the obtained results showed high variability and the assays were inaccurate. The use of signal amplification strategies with no prior studying of the kinetics could lead to such variations and inaccuracy. Moreover, the incubation time could be insufficient to bind molecules especially at very low analyte concentrations. This will lead to high variation and scattering of the obtained results due to non-specific signal amplification. Nevertheless, signal amplification cannot change the rate of the ligand-analyte biochemical interaction. Therefore, studying the kinetics will verify the binding of analyte molecules prior to applying amplification strategies and will lead to increasing the sensitivity, accuracy and reproducibility of the assay.
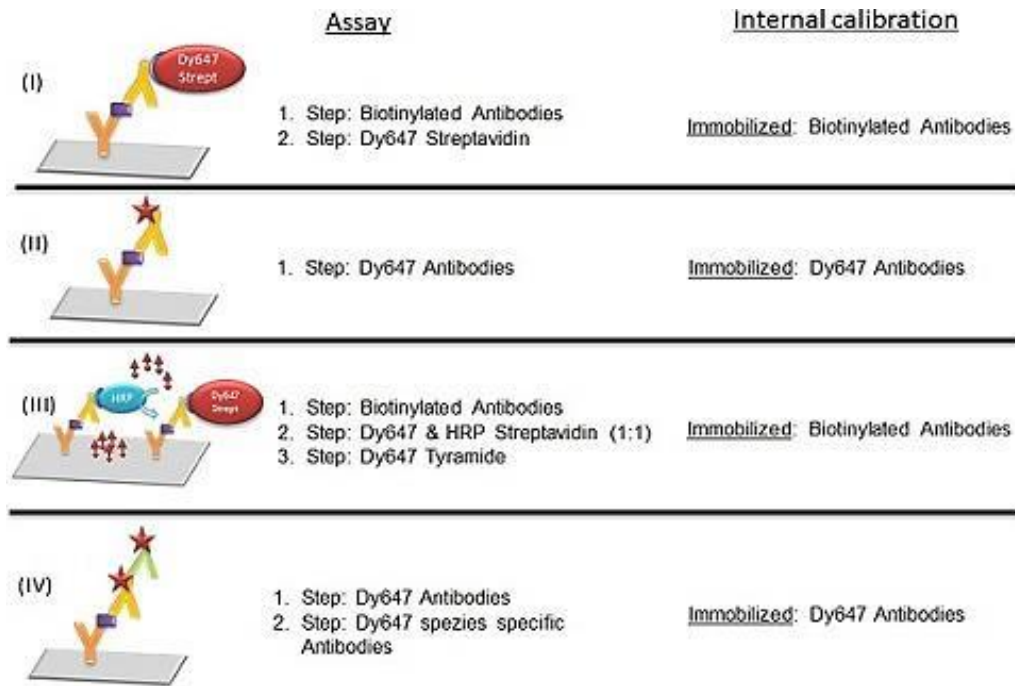
Figure 1.11 Schematic representation of the developed assays. The orange (Y): the capture antibody, the purple square: analyte, the yellow (Y) detection antibody, green(Y): labeled anti-detection antibody. Assay (I) used a biotin labeled antibody detected by fluorescently labeled streptavidin, (II) used an antibody directly labeled with a fluorophore, (III) used a biotin labeled antibody and enzymatic amplification by HRP and fluorescent tyramide, and (IV) used a labeled antibody to target the detection antibody (Buchegger and Preininger, 2014).

The same authors (Buchegger et al., 2012) earlier reported about a diagnostic microarray for neonatal sepsis. The microarray is capable of quantifying 9 various sepsis biomarkers. The assays showed up to 100-fold improvement in the sensitivity with increasing the incubation time from 1.5 hours to 2 hours after which there was no further or just slight improvement (Table 1). However, the authors did not discuss this effect and chose 2 hours as incubation time for their assays. The increase in the sensitivity with increasing incubation times could be well understood through studying the kinetics of the reaction. This will help to understand the type of limitations and their magnitude. Further, it could help deciding the proper design of the array and its ideal processing times.

Table 1 The assay processing times with the achieved limits of detection reported by Buchegger et al. (Buchegger et al., 2012).

Analyte	IL-6 (pg/mL)			S-100 (ng/mL)			E-Selectin (ng/mL)			CRP (µg/mL)		
Time (h)	2.5	2	1.5	2.5	2	1.5	2.5	2	1.5	2.5	2	1.5
LOD	1.1	1.2	149.0	0.7	1.8	5.0	4.0	6.3	30.1	0.10	0.27	0.48

Another work by Sauer and co-workers (Sauer et al., 2011) reports on the development of another sepsis diagnostic microarray. The authors combined two different assay formats on the same microarray to detect 7 of the low and high abundance sepsis biomarkers. Two different assay formats were used to detect low and high concentrations of biomarkers simultaneously. The processing time for this array was 4 hours. A rapid assay processed in 2.5 hours where the steps of incubation were combined to a single step was also developed. However, this assay was two orders of magnitude less sensitive. The authors explained that this effect is maybe due to the change of affinity to the analyte molecules due to their binding with the detection antibodies. However, the diffusion coefficient and subsequently the diffusion rate will most probably also be changed by this event. The change in the diffusion rate here would be due to the increase in the size and molecular weight of the analyte-detection antibody complex in comparison to the individual components. Moreover, the combination of the steps could additionally lead to a crowding of the buffer solution with molecules, a phenomena known as macromolecular crowding (Minton, 2001). This would as well affect the diffusion behavior compared to a less crowded buffer solution.

From the analysis of the previous examples, it is clear that achieving low limits of detection in short incubation times is the bottleneck for transferring microarrays from the laboratory to the routine diagnostic use. The discussed studies focused on changing the assay format to decrease both the limit of detection and assay processing time. However, microarrays based on highly affine capture molecules rely greatly on the diffusion of analyte molecules to the spots (Kusnezow et al., 2006a; Kusnezow et al., 2006c; Klenin et al., 2005). The introduction of high affinity capture molecules (monoclonal antibodies and aptamers) (Toh et al., 2015; Radom et al., 2013; Xu et al., 2010) and highly sensitive detection strategies (Gonzalez-Gonzalez et al., 2012; Berrade et al., 2011; Ray et al., 2010), therefore, did not yet provide the expected improvements in achieving high sensitivities within short assay times.

A clear understanding of the involved kinetics, therefore, would influence the choices made in designing a microarray and could lead to improvements. Yet, this issue is not well addressed in the literature especially for the novel 3D-hydrogel microarrays (Kusnezow et al., 2006a).

The introduction of 3D-hydrogel immobilization strategies improved the protein amounts immobilized on the surface and the achieved sensitivities in comparison with 2D microarrays (Moschallski et al., 2013). However, the kinetics involved has not been studied yet. Especially since the addition of a hydrogel matrix could influence the behavior of the molecules and affect the signal development, therefore, a kinetic investigation is urgently needed.

2. OBJECTIVES AND STRATEGY

As discussed in the previous chapters, microarrays still fail to deliver the expected sensitivities, i.e. the possibility to detect low analyte concentrations, at short incubation times. This is certainly one of the bottlenecks for transferring this technology to the routine diagnostics. To increase the sensitivity of microarrays the following strategies were applied in the literature (Buchegger and Preininger, 2014; Moschallski et al., 2013; Buchegger et al., 2012; Ramachandran et al., 2005):

1. Using complex chemistries to increase the amount of capture molecules on the surface.
2. Introduction of complex signal amplification strategies and highly sensitive sophisticated detection devices.
3. The use of high affinity capture molecules.

However, the previous strategies had very limited effects in terms of decreasing the incubation times. This is because microarrays rely greatly on the mass-transport of analyte molecules to the spots (Kusnezow et al., 2006a; Kusnezow et al., 2006c; Klenin et al., 2005). Yet, the kinetic processes involved in the signal development are not well characterized in the literature. The addition of a hydrogel matrix in 3D-hydrogel may affect the kinetic processes involved in the signal development. For these reasons, the following hypothesis was formulated: The understanding of the biochemical assay kinetics in 3D-hydrogel microarrays will lead to the better characterization and addressing of the imposed limitations.

2.1. OBJECTIVES

The aim of this work is to both characterize and understand the kinetics of biochemical assay in 3D-hydrogel microarrays described in details in section 1.2.2.2. Thereby the focus will be placed on determining the influence of diffusion onto the signal development. For molecules immobilized within the 3D-hydrogel matrix, the matrix may act as a diffusion barrier, which could represent a further limitation of the system. Therefore, this effect will also be studied.

2.2. STRATEGY

To study the effect of the mass transport on the kinetics of biochemical assay in 3D-hydrogel microarrays, high affinity systems should be used to exclude the affinity as a complex variable (Kusnezow et al., 2006a). In this work, biotin-streptavidin was the biological model of choice for studying the effect of mass transport on the assay kinetics in 3D-hydrogel microarrays.

First preliminary tests will be performed to determine suitable concentrations for the kinetic measurements using the attenuated total reflection (ATR) detection method. The suitable concentrations should be high enough to enable a real time measurement of the signals due to specific binding without washing steps. Additionally, it should allow reaching thermodynamic equilibrium within reasonable experimental times. Once these critical concentrations are determined, the kinetics of the biotin-streptavidin interaction on a microarray will be measured and compared to the existing model for biochemical kinetics in 2D-arrays (two-compartment model) (Figure 2.1) and the effect of mass transport will be determined. Additionally, the permeability of the hydrogel for proteins is studied using a model system. In this model, the microarrays are dip-coated with a thin uniform hydrogel layer prior to the kinetic measurements (Figure 2.2).
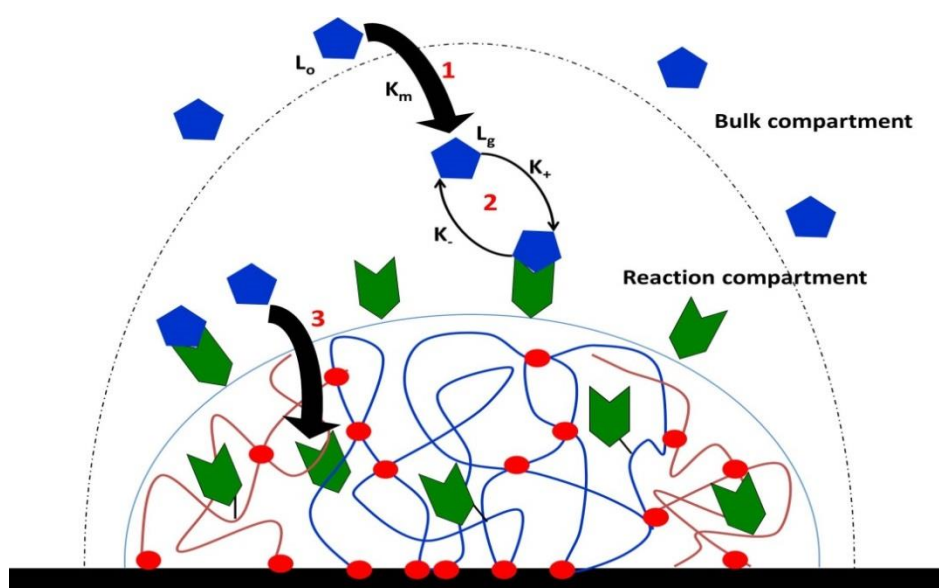
Figure 2.1 Schematic showing the kinetic processes involved in the processing of a microarray spot. 1) The mass transport kinetics based on the two-compartment model, the arrow represents the mass transport from the bulk compartment to the reaction compartment, and the dashed line represents the reaction compartment and 2) the arrows represent the binding reaction kinetics. 3) After time the capture molecules on the surface saturate and the analyte diffuse in the hydrogel layer to bind to capture molecules, the arrow represents the diffusion in the hydrogel layer. The blue symbols represent analyte molecules, green represents capture molecules, and the red dots represent cross-linking points.
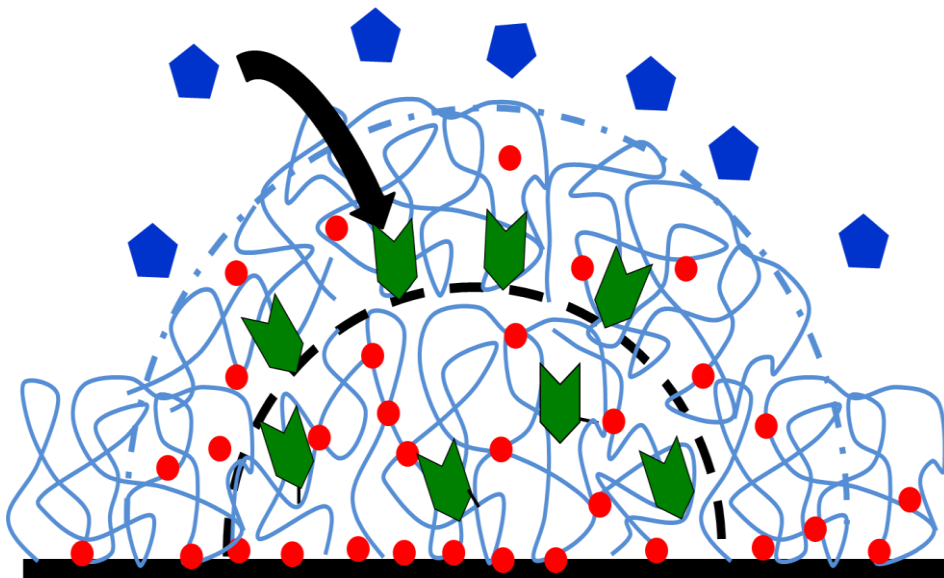
Figure 2.2 The developed model where the hydrogel coating on the microarray simulates the diffusion process in the hydrogel, process number 3 in (Figure 2.1). The arrow represents diffusion in the hydrogel coat to bind to molecules on the surface. The dashed line represent the spot. The blue symbols represent analyte molecules, green represents capture molecules, and the red dots represent cross-linking points.

3. THEORY

3.1. BIOCHEMICAL ASSAY KINETICS IN MICROARRAYS

3.1.1. REACTION LIMITED KINETICS

These reactions are limited by the binding event itself. Biochemical reactions can be described using the following general equation, which describes the binding/de-binding equilibrium (Kusnezow et al., 2006a; Rubina et al., 2005)

$$[L_o] + [R] \underset{k_-}{\overset{k_+}{\rightleftarrows}} [L_o.R]$$ 1.1.

With

- L_o: Concentration of the ligand (antigen) [M]
- R: Concentration of unoccupied receptor (antibody) [M]
- L_o.R: Concentration of the formed complex [M]
- k_+: Association rate constant $[Ms]^{-1}$
- k_-: Dissociation rate constant $[s^{-1}]$

The stability of the formed complex can be described by the dissociation constant as

$$K_d = \frac{k_-}{k_+}$$ 1.2.

With

- Kd: The dissociation constant [M]

K_d is a thermodynamic parameter that is used to describe the dissociation of the formed complex to its initial components. K_d values are also used to describe the affinity of biological pairs such as antibody-antigen pairs and DNA hybridization process, where smaller K_d values means higher affinity.

In an ideal assay, it is assumed that most of the limitations such as mass transport limitations, steric hindrance, and affinity heterogeneity are absent. The signal development over time can be described as:

$$S(t) = S_\infty \left(1 - \exp\left(-\frac{t}{\tau_{ideal}}\right)\right)$$ 1.3.

With

- $S(t)$: The signal developed after specific time t [a.u.]
- S_∞: Steady state signal intensity [a.u.]
- τ_{ideal}: The characteristic binding time of ideal kinetics [s] described as time needed for 63% of the reaction to complete

$$\tau_{ideal} = \frac{1}{(k_- + k_+ L_0)} \qquad \text{1.4.}$$

It is clear from equation 1.4 that there is an inverse relation between the ideal time of reaction and the initial analyte concentration, so increasing the concentration of the analyte leads to shorter characteristic binding time and vice versa. The rate of signal development in these assays depends on the association and dissociation rate constants of the system and the initial concentration of analyte.

3.1.2. MASS TRANSPORT LIMITED REACTION KINETICS

Protein-Microarrays were developed to detect specific target molecules typically a protein in a given sample. These assays usually make use of the biomolecular interactions or the biological activity of the molecule in question. For such interactions to take place, the molecules need to be in close proximity.

The analyte molecules travel in the solution by means of either diffusive or convective mass transport. Then the interaction between the analyte and the immobilized biomolecule takes place. Therefore, the biochemical assay can be described using the two-compartment model (Figure 3.2) (Kusnezow et al., 2006a) and can be broken down to two simple processes:

a) The mass transport process:

$$[L_o] \underset{K_m}{\overset{K_m}{\rightleftarrows}} [L_g] \qquad \text{1.5.}$$

With

- $[L_o]$: The concentration of the ligand in the bulk compartment [M]
- $[L_g]$: The concentration of the ligand in the reaction compartment [M]
- K_m: Mass transport constant [SU/Ms] is described as:

To derive an equation to describe the mass transport constant (K_m) kusneznow et al. (Kusnezow et al., 2006b) considered a totally absorbing disc of radius (R) covered homogeneously with antibodies of binding desnity (ρ) in this case the rate of absorption (K_s) is given by the Smoluchowski limit as

$$K_s = 4DRL_o$$

As the number of antibodies bound to antigens (N) increase by time:

$$N_{(t)} = K_s t$$

The signal development is

$$S_{(t)} = S_{max} \frac{N_{(t)}}{N_{max}}$$

Where N_{max} is the total number of antibodies available

$$N_{(max)} = \pi r^2 \rho$$

The signal development in a diffusion limited regime

$$S_{(t)} = S_{max} V_m t$$

Vm is the mass transport binding velocity

$$V_m = \frac{K_m L_o}{S_{max}}$$

Therefore from the previous considerations,

$$K_m = \frac{4DS_\infty}{\pi \rho R} \qquad\qquad 1.6.$$

With

- D: Diffusion coefficient of the analyte molecules [cm^2/s]
- ρ: The density of binding sites [mol/cm^2]
- R: Radius of the spot [cm]

b) The binding process:

$$[L_g] + [R] \underset{k_-}{\overset{k_+}{\rightleftarrows}} [L_o.R] \qquad \text{1.7.}$$

The signal development over time can be described as:

$$S(t) = S_\infty \left(1 - \exp\left(-\frac{t}{\tau_m}\right)\right) \qquad \text{1.8.}$$

With

- $S(t)$: The signal developed after specific time t [a.u.]
- S_∞: Steady state signal intensity [a.u.]
- τ_m: The characteristic binding time of mass transport kinetics [s] described as

$$\tau_m = \frac{S_\infty}{K_m K_d} \qquad \text{1.9.}$$

By substituting K_m in equation 1.10 with its description in equation 1.6 we get

$$\tau_m = \frac{\pi \rho R}{4 D K_d} \qquad \text{1.10.}$$

From equation 1.10, in a diffusion controlled system the characteristic binding time depends on:

1. Density of binding site (ρ) on the surface.
2. The radius of the spot.
3. Diffusion coefficient of the analyte in solution.
4. The dissociation constant (K_d).

In this model, the ambient analyte assumptions must be fulfilled:

1. The initial analyte concentration $[L_o]$ in solution is higher than the receptor $[R]$ concentration immobilized on the surface.
2. The amount of analyte depleted due to specific binding is small and can be neglected (Figure 3.1).
3. The receptor $[R]$ concentration is depleted due to specific binding.
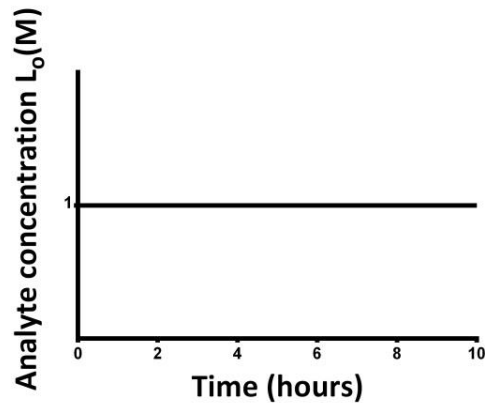
Figure 3.1 Plot of L_o as function of time showing the assumption of no analyte depletion due to specific binding over time.
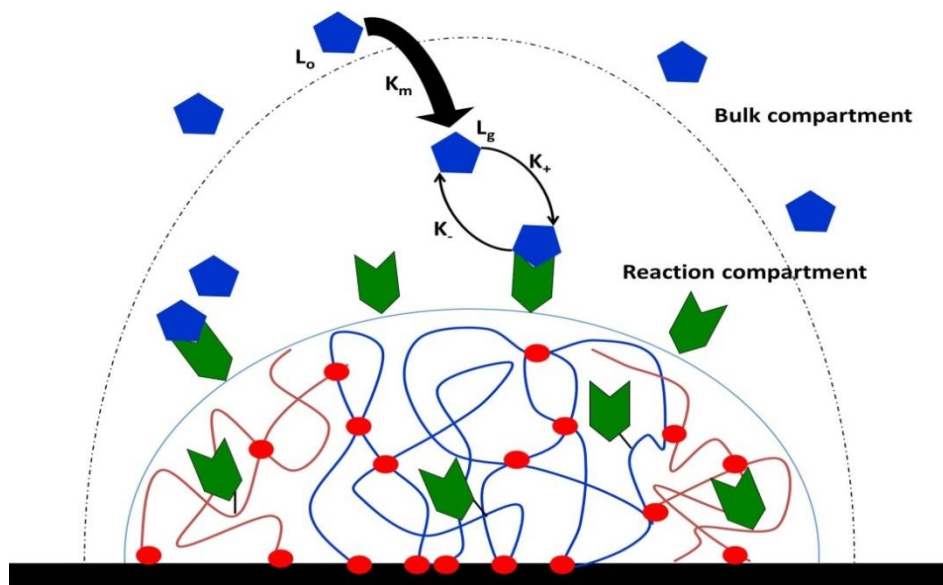
Figure 3.2: Schematic representation of the two-compartment model showing the two step reaction a) mass transport from bulk compartment (L_o) to the reaction compartment (L_g) and b) the binding reaction (Kusnezow et al., 2006a). The blue symbols are the analyte molecules, the green represent capture molecules immobilized on the surface, and the red dots are the cross linking points of the polymer.

3.1.3. Mass transport by diffusion

Diffusion is the movement of molecules down a concentration gradient following a Brownian movement and resulting in an even distribution of molecules in medium, this process was described by Adolf Fick in 1855 (Fick, 1995, 1855).

$$J = -D\frac{\delta c}{\delta x}$$ <div style="text-align: right">1.11.</div>

With

- J: The mass flux [mole/cm^2.s]
- D: The diffusivity [cm^2/s]
- C: is the concentration [M]
- X: The distance travelled by molecules [cm^2]

Under conditions of mass conservation, the time dependent formula of equation 1.11 is obtained

$$\frac{\delta c}{\delta t} = \nabla(D\nabla c)$$ <div style="text-align: right">1.12.</div>

Equation1.12 relates the change in the concentration to the mass flux to predict the change of the concentration as a function of time and can be written as

$$\frac{\delta c}{\delta t} = -\frac{\delta J}{\delta x} = \frac{\delta}{\delta t}\left(D\frac{\delta c}{\delta x}\right)$$ <div style="text-align: right">1.13.</div>

Based on Fick's laws of diffusion a model to calculate the time needed for diffusion can be derived. These assumptions must be fulfilled in order to use this model:

1. The initial receptor concentration is higher than the analyte concentration.
2. The affinity of the binding does not limit the reaction.
3. The analyte concentration is depleted due to specific binding.

Imagine a spot of capture molecules with concentration $[R_o]$ printed in the center of an incubation chamber with length [L], width [W], and height [H] (Figure 3.3). The maximum distance an analyte molecule has to diffuse $[X_{max}]$ to the centered spot is:

- Half the length of the chamber [L]/2 denoted by [a]
- Half the width of the chamber [W]/2 denoted by [b]
- The height of the chamber [H] denoted by [c]

$$X_{max} = \sqrt{a^2 + b^2 + c^2}$$ 1.14.
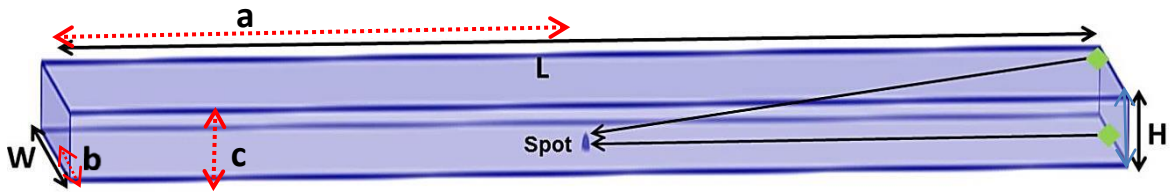
Figure 3.3 Schematic showing the dimensions of the incubation chamber and the location of the spot in the center. The furthest analyte molecules within the chamber are shown in green.

The array is incubated with analyte concentration $[C_o]$ such that $[C_o] << [R_o]$ and the reaction is divided into two phases:

a) Depletion phase:

Initial analyte concentration in the solution is $[C_{(t)}] = [C_o]$ and the distance travelled by the molecule $[X_{(t)}] < [H]$. The reaction proceeds and the initial $[C_o]$ is depleted due to specific binding. This phase can described using the following equations according to Fick's first equation 1.11:

$$J = -D\frac{C_o}{X_t}$$ 1.15.

Number of analyte molecules [n] at time [t] in the incubation chamber:

$$n_{(t)} = HC_o - \frac{1}{2}X_{(t)}C_o$$ 1.16.

$$\frac{\delta n}{\delta t} = J$$ 1.17.

$$-\frac{1}{2}\frac{\delta X_{(t)}}{\delta t}C_o = -D\frac{C_o}{\delta X_{(t)}}$$ 1.18.

27

$$X_{(t)} = \sqrt{4Dt}$$

<div align="right">1.19.</div>

The depletion phase ends when $X_{(t)}$ = H therefore the time needed for this phase is:

$$t_1 = \frac{H^2}{4D}$$

<div align="right">1.20.</div>

b) Linear phase:

When the analyte molecules are significantly depleted $[C_{(0,t)}] < [C_o]$ then the following equations apply:

$$n_{(t)} = \frac{1}{2} X_{(t)} C_{(o,t)}$$

<div align="right">1.21.</div>

$$\frac{\delta n}{\delta t} = J$$

<div align="right">1.22.</div>

$$\frac{1}{2} X_{(t)} \frac{\delta C_{(o,t)}}{\delta t} = -D \frac{C_{(o,t)}}{\delta X_{(t)}}$$

<div align="right">1.23.</div>

$$C_{(o,t)} = C_o \exp(-\frac{2D}{X_{(t)}^2} t)$$

<div align="right">1.24.</div>

By taking the natural logarithm for both sides

$$t_2 = \frac{X_{max}^2}{2D} \ln\left(\frac{C_o}{C}\right)$$

<div align="right">1.25.</div>

3.1.4. DEPLETION ZONES FORMATION

A characteristic phenomenon of the solid phase immunoassays is the formation of depletion areas around the immobilized capture molecules. The binding event of analyte molecules decreases the amount of free analyte molecules in the solution. As a result, areas where the analyte molecules are depleted are formed around the capture molecules expanding as the incubation time increase as shown in (Figure 3.4) (Bönisch, 2008).

The distance a molecule travels in a specific time is defined by the Einstein-Smoluchowski equation (one dimension diffusion) as the following (Bönisch, 2008)

$$X^2 = 2Dt \qquad\qquad 1.26.$$

The diffusion coefficient of streptavidin used throughout this thesis is 1.3×10^{-6} cm^2/s (Zhang et al., 2007), thus the time required for diffusing over a distance of 1mm is almost 1 hour in aqueous solutions.
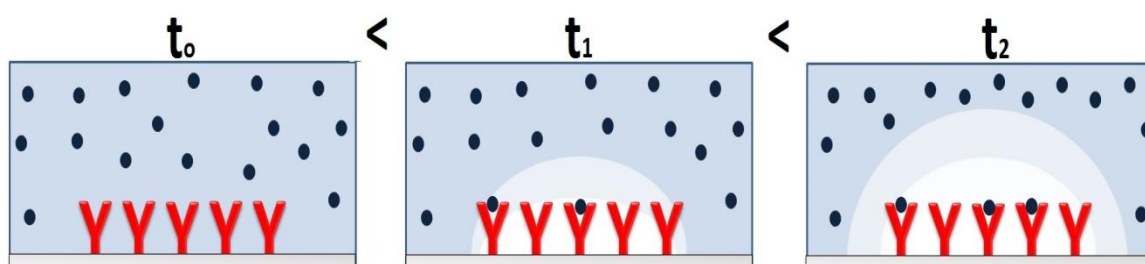
Figure 3.4 Schematic representation for the formation of depletion zones with increasing the incubation time (Bönisch, 2008). At t_o the free analyte molecules are randomly distributed in the solution, after time = t_1 ($t_1 > t_o$) the binding event causes the depletion of the free analyte molecule and a depletion zone starts to form and at time = t_2 ($t_2 > t_o$) more binding of analyte caused increase in the depletion zone. The red (Y) represent the capture molecules, blue spots represent the analyte molecules and the light shades of blue represents depletion zones (areas depleted from analyte molecules).

3.2. HYDROGELS

Hydrogels are 3D cross-linked polymers of hydrophilic nature; they swell by absorbing water while staying insoluble in aqueous media due to the physically or chemically induced cross-linking of the polymer chains (Buenger et al., 2012; Lin and Metters, 2006).

According to Peppas and co-workers (Peppas et al., 2000), three parameters govern the nanostructure of a hydrogel network (Figure 3.5).

1. The polymer volume fraction in swollen state ($V_{2,s}$).

2. The number average molecular weight between cross-linking points ($\overline{M}_c$).

3. The mesh size of the network (ξ).
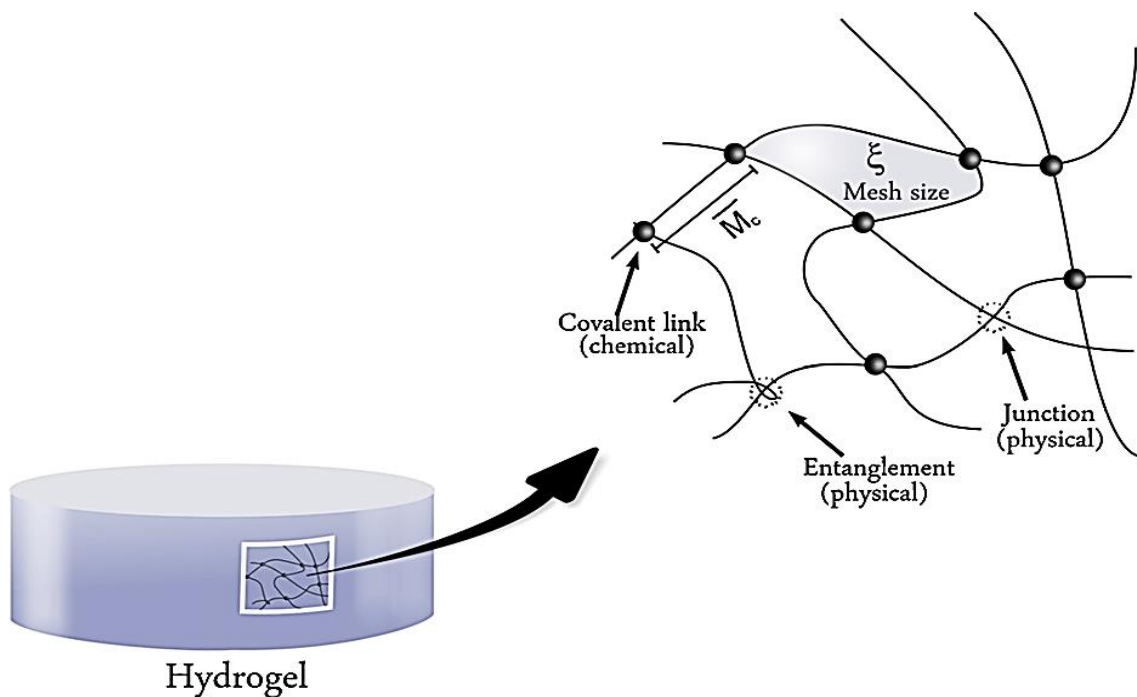
Figure 3.5 Schematic showing the mesh size (ξ) and the average molecular weight between cross-linking points ($\overline{M}_c$) (Buenger et al., 2012).

The polymer volume fraction in the gel (swollen state) $\left(V_{2,s}\right)$ describes how much liquid can be absorbed by the hydrogel resulting in swelling. It is the ratio of the polymer volume in the dry state $\left(V_p\right)$ to the volume of the swollen gel $\left(V_{gel}\right)$

$$V_{2,s} = \frac{V_p}{V_{gel}}$$ 1.27.

The number average molecular weight between two cross-linking points $(\overline{M}_c)$ describes the true level of cross linking and is described as

$$\overline{M}_c = \frac{M_o}{2x}$$ 1.28.

With

- M_o : The molecular weight of repeating monomeric units
- x: The degree of cross-linking

Higher cross-linking degrees are associated with an increase in the mechanical strength and a decrease in the diffusion rate due to the decrease in the mesh size of the network (ξ) (Gauthier et al., 2004).

The mesh size of the network (ξ) indicates the distance between two cross-linking points, and defines the space available for diffusion of molecules through the matrix. It is described as (Nicodemus and Bryant, 2008; Lin and Metters, 2006)

$$\xi = V_{2,s}^{-1/3}(\overline{r_0^2})^{1/2}$$ 1.29.

With

- $(\overline{r_0^2})^{1/2}$: The root-mean-squared end-to-end distance of network chains between two adjacent cross-links in undisturbed state.

3.2.1. DIP COATING

The dip coating process enables the deposition of a uniform film on the surface of a substrate. The surface is immersed into a solution for a period of time to allow the full wetting of the surface then the substrate is withdrawn from the solution at a predetermined speed allowing the solvent to evaporate leaving behind a uniform film of coating (Figure 3.6) (Yimsiri and Mackley, 2006).

The major forces governing the process are viscous drag, gravitational force, capillary force and inertia force (Schunk et al., 1997).

$$h_o = 0.944 \frac{(\eta u_o)^{2/3}}{\sigma^{1/6}(\rho g)^{1/2}} = 0.944(Ca)^{\frac{1}{6}}\left(\frac{\eta u_o}{\rho g}\right)^{1/2} \qquad 1.30.$$

With

- h_o: The film thickness [m]
- η: The viscosity of the solution [kg/m.s]
- u_o: The withdrawal speed [m/s]
- σ: The surface tension of the solution [N/m]
- ρ: The density of the solution [kg/m^3]
- (Ca): Capillary number = $\frac{\eta u_o}{\sigma}$
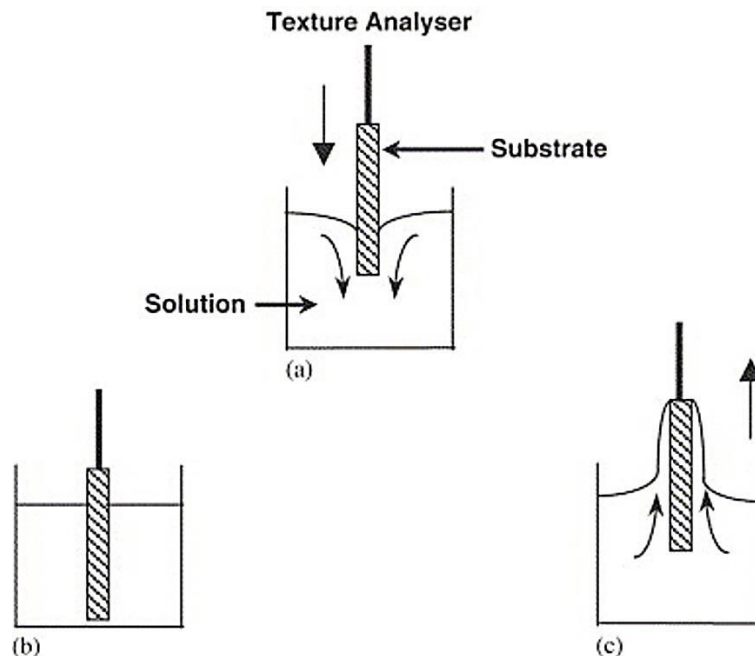
Figure 3.6 Schematic representation of the dip-coating process. (a) Substrate immersed in solution, (b) wetting of the substrate, and (c) withdrawal at constant speed (Yimsiri and Mackley, 2006).

4. MATERIALS AND METHODS

4.1. MATERIALS

4.1.1. BIOLOGICAL SPECIES

In this work biotin-streptavidin system was the biological system of choice, the high affinity of the system enables strong and reproducible signal development. Moreover, it removes the affinity as a complicated variable and allows the study of the diffusion behavior.

> Name: Streptavidin, cy5 conjugate
> Supplier: GE Healthcare UK Ltd, England
> Molar mass: 60 kDa
> Concentration: 1 mg/ml
> Diffusion coefficient: 1.3×10^{-6} cm^2/s (Zhang et al., 2007)
> Hydrodynamic radius: 2.5 nm (Swift et al., 2006)

A corresponding biotin labeled oligonucleotide was used as a capture molecule, the oligonucleotide acts as a spacer for the immobilized biotin molecules

> Name: Biotinylated-oligonucleotide
> Supplier: TIB MOLBIOL, Berlin, Germany
> Size: 24-mer
> Sequence: BIOTEG-TgCgTCAAAggTgTTTTTTTTTTTT
> Concentration: 100 μM

4.1.2. MICROCHIP SUBSTRATES

The standard microchip substrate used throughout this thesis is polymethylmetacrylamide (PMMA) supplied by form.in displays Laser-Center GmbH, Heitersheim, Germany.

All substrates were in the standard microscope slide format of 25 x 75 x 1 mm^3.

384 wellplates were obtained from Genetix, New Milton, UK.

Gene frame seals and the cover slips with a volume of 65μl and dimensions of 1.5x1.6 cm were supplied by Fisher Scientific - UK Ltd.

4.1.3. POLYMERS USED FOR THE 3D-HYDROGEL IMMOBILIZATION

As described in section 1.2.2.2 the immobilization technique used throughout this thesis depends on a 3D-hydrogel network consisting of the following

PDMAA polymer with Styrene-4-sulfonic acid sodium salt (SSNa) as additive shown in (Figure 1.9 A) was synthesized using standard free radical polymerization process (Rendl et al., 2011)

Backbone: PDMAA
Crosslinker: 5 mol% MABP
Additive: 2.5 mol% Styrene-4-sulfonic acid sodium salt (SSNa)

4.1.4. POLYMERS USED FOR COATING THE CHIPS

A novel model where the microarrays were coated with a hydrogel layer after the manufacturing process allows for the study of the diffusion through the hydrogel.

Here different amount of crosslinker were used to change the mesh size of the resulting hydrogel layer.

Backbone: PDMAA
Crosslinker: 5 mol% MABP or 1 mol% MABP
Additive: 2.5 mol% Styrene-4-sulfonic acid sodium salt (SSNa)

4.1.5. CHEMICAL REAGENTS AND LABORATORY EQUIPMENT

Chemicals used throughout this work were purchased from standard suppliers and used without further purification. A list of chemicals and used laboratory equipment can be found in the appendix.

4.2. METHODS

4.2.1. FABRICATION OF THE MICROCHIPS

4.2.1.1. PREPARATION OF THE SLIDES

Briefly, the microchips are cleaned in a 1:1 ethanol water mixture in ultra-sonic bath for five minutes. Afterwards, the slides were rinsed thoroughly with DI water and dried in a centrifuge at 2500 rpm for at least five minutes.

4.2.1.2. PREPARATION OF THE PRINTING SOLUTION

The solutions containing the biological species were pipetted into a 384 wellplate, the final volume per well was 40 µl. First, a polymer solution (10 mg/ml polymer in nuclease free water) was prepared, then the corresponding bioactive species were suspended in the wells using a sodium phosphate buffer (NaPi) of 100 mM and 4 µl polymer solution was added, resulting in a final polymer concentration of 1 mg/ml.

4.2.1.3. PRINTING PROCESS

Printing of the microarrays was done using a S3 Sciflex contactless arrayer, (Scienion, Berlin, Germany). It consists of a printing head movable in three axes, a glass capillary for dispensing solutions surrounded by a piezo crystal referred to as "nozzle", a plate holder for the 384 well microtiter plate, slide holder for placing the chips to be printed, and two CCD cameras for controlling the process.

The printing solution is dispensed out of the nozzle in form of drops by the pulse contraction of the piezo crystal. The drop volume can be adjusted precisely by changing the pulse width and voltage of the signal triggering the piezo actuator as shown in (Figure 4.1).

The quality and the volume of the drop are automatically controlled by the print software before and after each individual probe is spotted, to ensure the quality and homogeneity of the produced arrays.

Due to the contactless spotting process, the dispensed volume is not affected by the roughness, surface tension, and hydrophobicity of the printing surface itself. The drop volume was 345 $\pm$ 5 picoliter with relative humidity of 50 $\pm$ 2 % and temperature 24 $\pm$ 2 °C. 4 drops were printed per each spot (1.38 nanoliter).
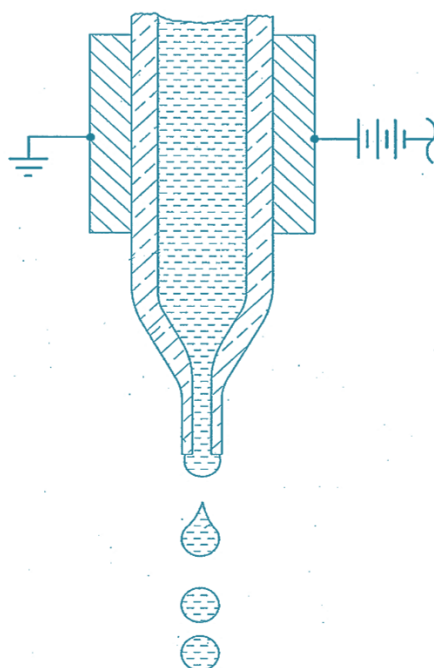
Figure 4.1 Schematic showing the nozzle of the printer with the piezo crystal surrounding it and controlling the drop size through the charge (Tisone and Eickhoff, 2013).

4.2.1.4. CROSSLINKING

As mentioned in section 1.2.2.2, the printing process was followed by a brief exposure to a UV-light to photocrosslink the hydrogel. For this purpose a Stratalinker 2400, from Stratagene, La Jolla, Ca, USA, was used with crosslinking energy of 1.5 J/cm^2 at a wavelength of 254 nm.

4.2.2. DIP COATING

After the immobilization process, the microarrays to study the diffusion in the hydrogel were dip-coated using a Z 2.5 tension-testing machine from Zwicki GmbH. The precursor polymer solutions with concentrations 1, 5 and 10 mg/ml were prepared in ethanol. The microarray slides were immersed in the solution at ambient room temperature and pulled at a velocity of 50 mm/min.

The dip-coating process was followed by a UV-exposure at a wavelength of 365 nm with crosslinking energy of 3 J/cm^2, resulting in a thin layer of hydrogel covering the microarrays.

4.2.3. INCUBATION

Prior to incubating the microarrays, they were briefly washed with ethanol water mixture for a period of 5 minutes.

The microarrays were incubated using the gene frame seals with capacity of 65 μl. Streptavidin cy-5 was diluted in PBST solution at a concentration of 19 nM (1 μg/ml, 7.44 x 10^{11} molecules / 65 μl) and the incubation time was at least 3 hours.

4.2.4. Fluorescence detection and readout of the microarrays

After incubation, the microarrays were analyzed. The reaction is detectable through the fluorescence signal emitted by the cy5 label attached to the streptavidin. Upon excitation by an incident light of a specific wavelength, the fluorophore absorbs the incident photons and emits photons and a lower energy and of a higher wavelength. In this case, the excitation wavelength is 640 nm and the emission is 670 nm, this phenomenon is known as Stokes shift.

4.2.4.1. ATR microarray reader

To allow for the time resolved kinetic measurement of the microarray a readout device that would allow the acquisition of a serious of images over a period of several hours is necessary. A detection device based on attenuated total reflection (section 1.2.3.1) was used (Figure 4.2). The device is controlled by a script containing the exposure time and time intervals for capture. The exposure time used for the measurements of the assay kinetics was 20 seconds.
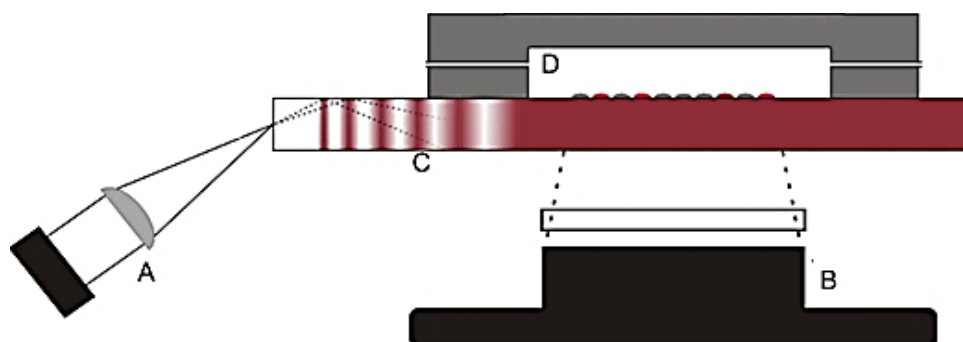
Figure 4.2 Schematic drawing showing the components of the ATR, A) laser, B) CCD camera, C) microarray slide and D) flow cell (Rendl, 2009).

4.2.4.2. Imaging and data analysis

Analysis of the 16-bit grey scale images obtained from the ATR was done using the imaging software Signalyse™ (Holger Klapproth life science). After defining a grid with the printed array pattern, the spots are analyzed by a pattern recognition algorithm. Misshaped or misplaced spots are discarded from the evaluated data automatically. The software's output is either a file with single spots each assigned with its signal intensity or a library with mean and standard deviation for a probe with more than one identical spot on the same array.

4.2.5. DESIGN OF EXPERIMENTS

This section describes the experimental considerations that were taken into account to guarantee the reproducibility and significance of the obtained data.

4.2.5.1.   REDUNDANCY

Throughout the experiments done during this work, on chip redundancy of at least 12 identical spots per parameter to account for the variability and to represent a conclusive result with respect to scattering of the measured signals. Additionally, each experiment was repeated at least two times to assess both reproducibility and inter-array variation.

4.2.5.2.   CONCENTRATION OF BIOLOGICAL SPECIES

The concentration of the coupling control (streptavidin-cy5) was fixed at 5 µM, this showed no interference with the readout of the arrays and the low intensities of the bound analyte molecule were detectable.

To have a representative range and assess the effect of varying the concentration on the kinetics, the concentration of the biotin-oligonucleotide was varied from 10, 5 and 1 µM. These concentrations correspond to 8.19×10^9, 4.1×10^9 and 8.19×10^8 molecules per spot respectively. The total number of capture molecules on the microarray was 9.4×10^{10}.

The concentration of the analyte solution (streptavidin cy-5) was 19 nM or 1 µg/ml (7.44×10^{11} molecules / 65 µl) for all the experiments. The concentration of the analyte was one order of magnitude higher than the total amount of the capture molecules per microarray.

4.2.5.3.   INCUBATION TIME

The incubation time was 3 hours in a static incubation. Preliminary experiments showed that a state of equilibrium is reached within that period for the concentration of capture molecules and analyte used in this thesis.

4.2.5.4.   PRINT LAYOUT

The assay layout allowed the investigation of the possible signal variation between spots due to the individual spot position on the array. Using this print design allowed the detection of effects such as the presence of air bubbles or uneven distribution of the analyte within the seal frame. The diameter of the spots was about 250 µm and the inter-spot distance was 750 µm as shown in (Figure 4.3). Spots consisting of NaPi buffer and polymer with no biological species (negative control) were printed to detect and quantify unspecific binding.
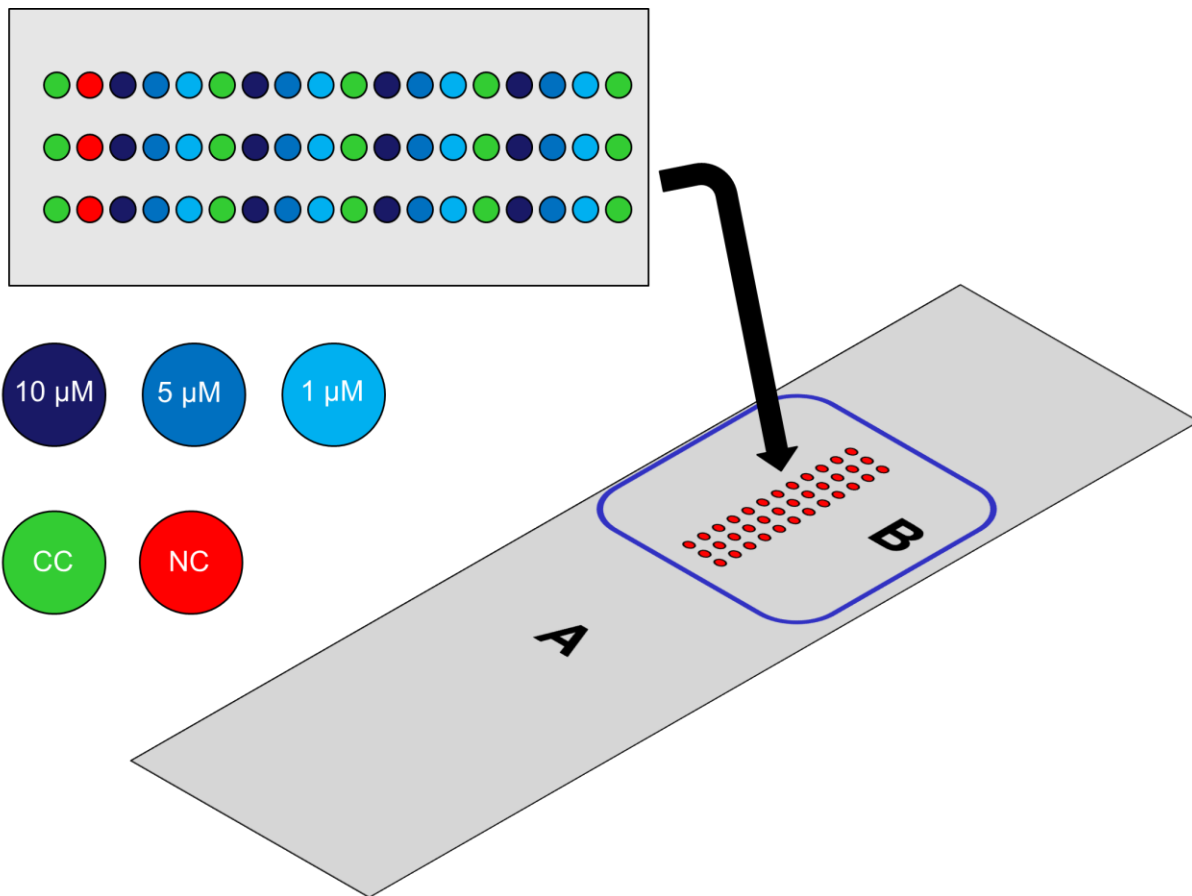
Figure 4.3 Schematic illustration of the microarray layout used throughout this thesis. (A) Represents PMMA microscopic slide with a microarray and (B) is the print area showing the array. (CC) is coupling control (Cy5 labeled streptavidin), (NC) is the negative control (polymer with no biological species,) and (10 µM, 5 µM, and 1 µM) are the concentrations of biotin-oligonucleotide in the designated spots. The inter-spot distance was 750 µm and the spot diameter is 250 µm.

5. RESULTS AND DISCUSSION

5.1. MICROARRAY DESIGN, PRINTING AND PROCESSING

First, the appropriate concentration range for measuring the assay kinetics using the ATR detection method had to be determined. Microarrays were printed with varying surface density of fluorescently labeled oligonucleotide to assess the detection limits of the device. A Cy5 labeled oligonucleotide was used due to its known degree of labeling (1:1). This simplifies calculating the detection limits as for the measurement technique used. Additionally, they act as a spacer for the immobilized functional molecule assuring that the conformational structure is preserved for the protein. The used concentrations were in the range of 0.000027 µM to 2.7 µM (2 nanoliter per spot with radius of 250 µm). Three different exposure times were used 10, 20, and 30 seconds. The fluorescence intensity of the microarrays was measured in the dry state and during the incubation with fluorescently labeled streptavidin with concentrations ranging from 0.5 nM to 500 nM. This allowed determining the limit of detection in the presence of fluorescent background. In the dry state, the ATR was able to detect the 0.0027 µM of Cy5 labeled oligonucleotides. This corresponds to 10 fluorophores/µm^2 when the degree of labeling of oligonucleotide-cy5 (DOL = 1) and the immobilization efficiency of the 3D-hydrogel (60 %) are taken into account (Figure 5.1) (Rendl et al., 2011; Rubina et al., 2003).
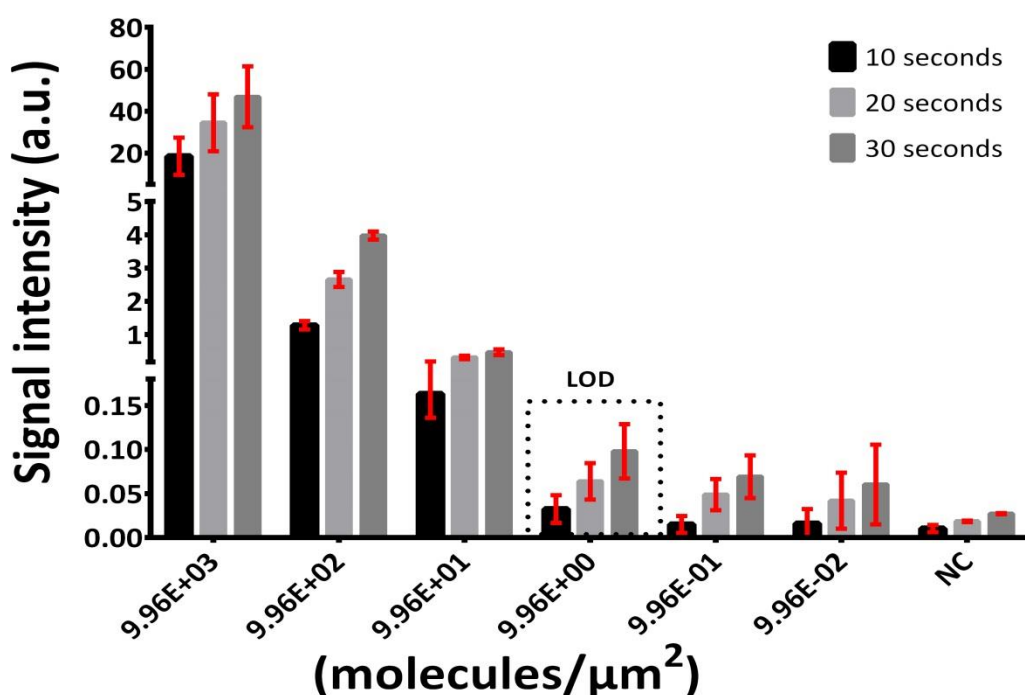
Figure 5.1 The obtained signal intensities for the microarrays in the dry state with different exposure times (10, 20, and 30 seconds). Plotted the number of fluorophores/μm^2 for the used concentration range (2.7, 0.27, 0.027, 0.0027, 0.00027 and 0.000027) and the negative control ((NC) spots containing polymer in print buffer without biological species. The insert shows limit of detection (LOD) corresponds to approximately 10 fluorophores/μm^2.

However, the presence of fluorescent solution strongly affected this sensitivity value quite strongly. In this case, the sensitivity of the device decreased by two orders of magnitude and only 1000 fluorophores/μm^2 could be detected when incubating with 0.5 and 5 nM streptavidin Cy5 solution. In the case of 50 nM, the limit of detection dropped by three orders of magnitude (Figure 8.1, Figure 8.2 and Figure 8.3).

It was observed that the exposure time is also critical for measuring the kinetics. A compromise had to be made between short time intervals between the measurements and relatively higher sensitivities. 20 seconds was chosen as the exposure time for the kinetic measurements as it showed low scattering of measurements (SD: 10 %) and acceptable signal to background ratio of 5.

Moreover, higher amounts of immobilized biotin molecules (1, 5 and 10 µM of biotin labeled oligonucleotide in the printing solution) were chosen for having higher specific signals that could be quantified with no interference of the background (signal to background ratio≥ 3). Furthermore, the optimal concentration of the analyte (streptavidin Cy5) had to be determined for measuring the kinetics. Therefore, the microarrays were incubated with varying concentrations of streptavidin-Cy5 (0.1, 1 and 2 µg/ml) and the signal development

over time was recorded. The most suitable concentration was found to be 1 μg/ml. In the case of 0.1 μg/ml the assay kinetics was very slow, and on the other hand for 2 μg/ml the signal development was too fast for the ATR to resolve. Based on these findings, the conditions for the assay kinetics study were derived (1 μg/ml streptavidin cy5 solution and 1, 5 and 10 μM immobilized biotin labeled oligonucleotides). The designed arrays consisted of 12 spots for each concentration of biotin labeled oligonucleotides in 4 sub arrays (Figure 5.2.b). To mark the start and the end of the sub arrays, coupling control spots (Cy5 oligonucleotides) were included and for evaluation of non-specific binding negative control spots (polymer in print buffer containing no oligonucleotides) were used (Figure 5.2.b).

Figure 5.2 a) False color image of the designed microarray after processing. The scale bar indicates the inter spot distance of 750 μm. b) the print scheme of the array, the green spots represent the coupling controls (oligo-Cy5), the red spots are the negative control (polymer without oligonucleotides), and the blue spots represent 10, 5 and 1 μM biotin labeled oligonucleotides.

5.2.   KINETIC STUDY OF 3D-HYDROGEL MICROARRAYS

The arrays presented in the previous chapter were used for the kinetic measurement. The microarrays were printed, processed, and incubated with 1 μg/ml streptavidin-Cy5 in a PBST buffer. The arrays were analyzed in the ATR-setup and a sequence of 160 images was acquired over a period of 15 hours with an exposure time of 20 seconds each. The assay mentioned here represented a direct non-competitive immunoassay. The data were compared to the two-compartment model and to ideal reaction kinetics with no limitations. The fittings to the model were done using nonlinear least squares fitting method (Brown, 2001). The quality of the fit was analyzed using two parameters the coefficient of determination (r^2) and reduced Chi squared (x^2). The measured assay kinetics and the comparison to the model (for two different fitting parameters) are shown in (Figure 5.3).
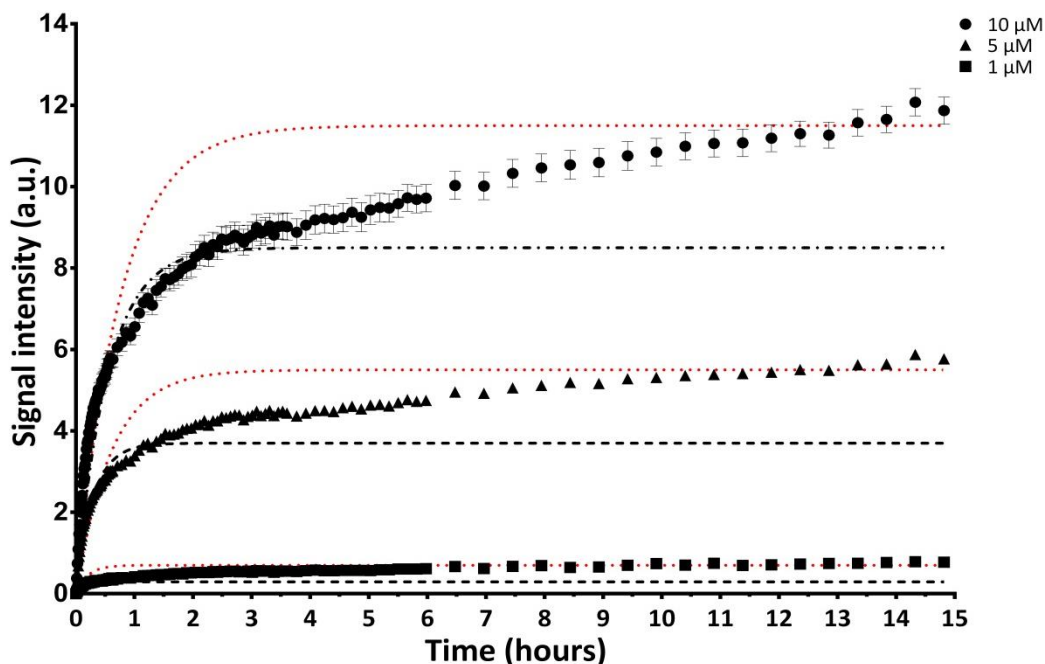
Figure 5.3 Observed biotin-streptavidin assay kinetics using the 3D-hydrogel microarrays. Three different spotting concentrations for biotin incubated with 1 µg/ml streptavidin-cy5 are shown. The data points represent the average of 12 spots and the error bars indicate the standard error. The lines represent the possible fittings of the two-compartment model.

From analyzing the kinetic data in (Figure 5.3), it was observed that the initial phase is linear and reflects the change in analyte concentration over time which agrees with the expected curves. The second phase was expected to be exponential with a steady state signal saturation. However, this was not seen and the signal was still increasing over time with a slower rate of reaction.

Two possibilities were obtained by fitting the two-compartment model to the data. The first was to fit the data using the maximum measured signal for the kinetic curve (dotted red lines Figure 5.3) and the other was to fit the model so that optimum agreement was achieved in the first part of the curve (dashed black lines Figure 5.3). Both fittings showed good agreement in the first phase.

To confirm the agreement of the two-compartment model with the initial phase in the observed kinetics, the measurement time was decreased to 3 hours. This time is sufficient to determine whether the experimental data deviates from the two-compartment model in the initial phase.

The fluorescence intensities were analyzed in the ATR-setup and a sequence of 124 images was acquired over a period of 3 hours with an exposure time of 20 seconds each (the measuring rate was increased to check for the point of deviation from the model). The two compartment model was fitted to the data ($r^2 = 0.968$, $X^2 = 0.002$) and the characteristic mass transport binding time ($T_m = 0.45$ hours) was derived from the fitting (Figure 5.4).
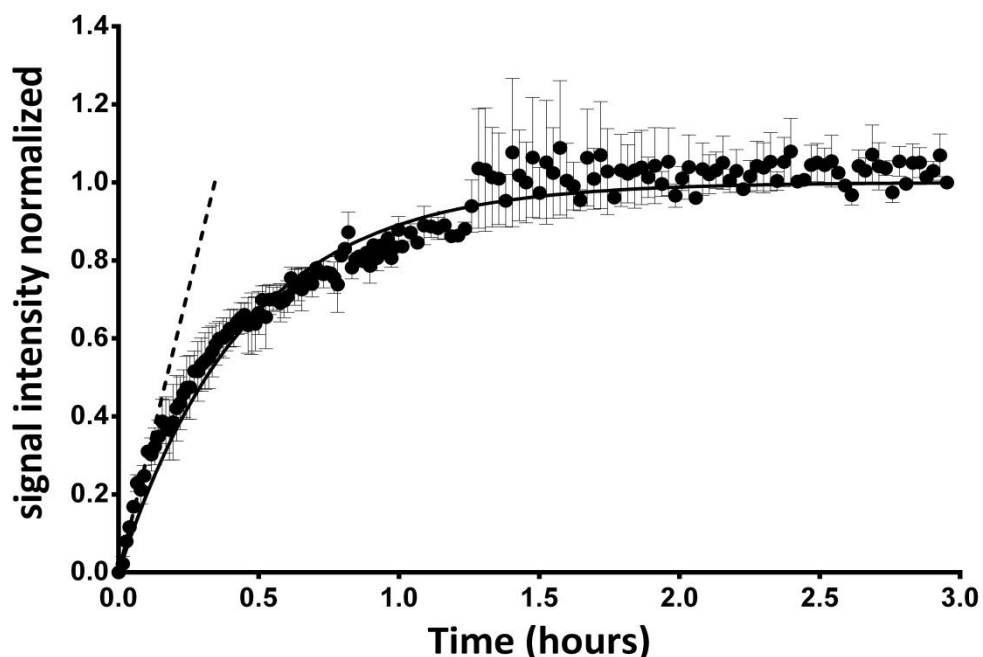
Figure 5.4 Measured biotin-streptavidin assay kinetics using the 3D-hydrogel microarrays for 3 hours. The data points represent the normalized average signal for 10 μM biotin oligonucleotides of the 2 chips with on chip redundancy of 12 spots. The solid line represents the fitting according to the two-compartment model $r^2 = 0.968$, $X^2 = 0.002$. The dashed line represents the linear regression analysis of the first 10 data points $Y = 2.82X$, $r^2 = 0.964$. The error bars represent the standard error.

The obtained data for the highest biotin concentration on the surface (10 μM) were normalized to the maximum signal obtained after 3 hours. From the analysis of the kinetic data in (Figure 5.4) very good agreement and fitting with the two-compartment model was observed. The curve obtained could be divided to two phases, the initial phase which is linear and represents the binding rate depending on the mass transport and the second exponential phase represents the steady state approximation. This confirms the suitability of the two-compartment model to describe the initial part of the assay kinetics observed.

Based on these results, the two-compartment can be used to describe the initial parts of the kinetic curves obtained (Figure 5.3). Accordingly, the data points included in the fitting were adjusted. For the 10 μM the model agreed with the first 80 data points ($r^2 = 0.975$, $x^2 = 0.36$), for the 5 μM the first 60 data points showed agreement ($r^2 = 0.979$, $x^2 = 0.04$) and for the 1 μM the first 35 points ($r^2 = 0.971$, $x^2 = 0.00021$).

To confirm the mass transport dependence of the measured kinetics, the data were compared to an ideal reaction depending on the association rate constant (k_+), the dissociation rate constant (k_-) and the initial analyte concentration (L_o). The calculated ideal binding time (T_{ideal}, time need for 60% of the reaction to complete) was 0.7 seconds, three orders of magnitude lower than the observed kinetics. In a mass transport limited system, the characteristic binding time (T_m) depends on the concentration of the immobilized capture molecules. According to equation (1.10), the relation between the characteristic mass transport binding time (T_m) and the concentration of capture molecule is linear. This was confirmed by plotting the characteristic mass transport time (T_m) versus the concentration of the capture molecules. A linear relation, which is in good agreement with the theory, was observed (Figure 5.5).
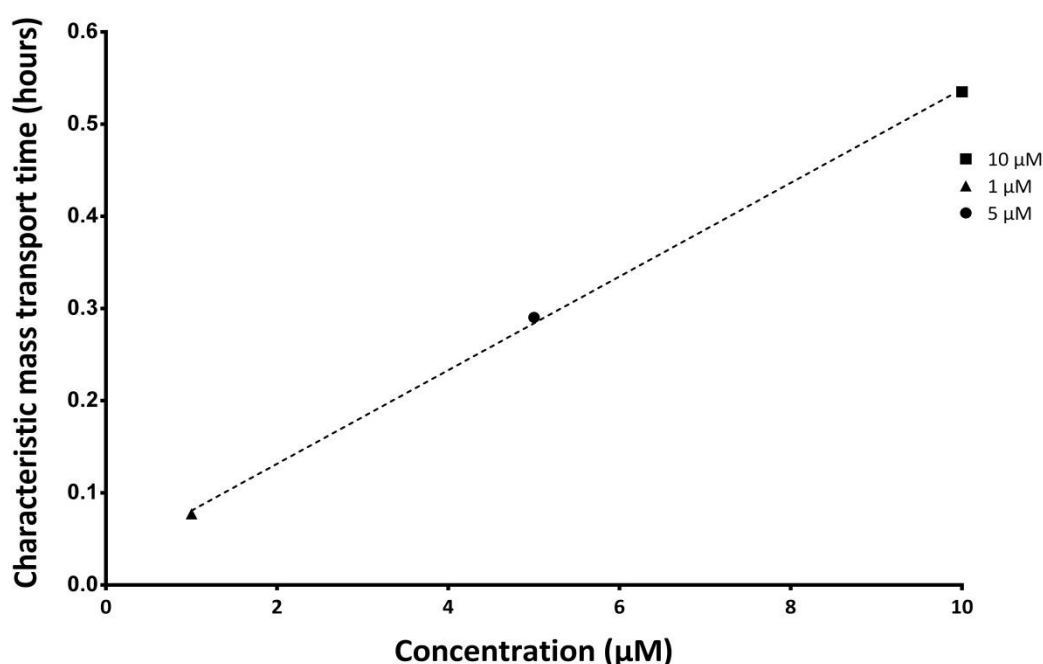
Figure 5.5 plotted characteristic mass transport binding time (Tm) versus the concentration of biotin printed on the surface $Y = 0.05079X + 0.03007$, $r^2 = 0.9994$.

The measured assay kinetics (Figure 5.3) was compared to the two-compartment model, which was developed to describe the kinetics of biochemical assays in 2D hydrogel microarrays. It showed very good agreement in the initial phase as can be seen from the kinetic curves in (Figure 5.3). However, a deviation from the model was observed in the second phase that needs to be addressed. This deviation could be attributed to:

1. Deviation from the assumption of a non-depleting supply of analyte (L_o)

The analyte concentration should not be depleted due to specific binding, as the fraction of bound molecules is so small and can be neglected. However, analyte molecules could also be lost by nonspecific adsorption to the surface itself. This could be addressed by increasing the

initial amount of analyte. This was not possible experimentally due to the very high fluorescent background that hindered the quantification of specific signal due to binding (signal to background ratio $\geq$ 3). The change in the analyte concentration would change the mass transport rate and consequently the rate of the signal development.

The built-up of a depletion zone would limit the analyte diffusion and will then change the mass transport behavior. This will cause a change in the distance analyte molecules have to travel through the solution decreasing the reaction rate significantly.

However, the depletion of the analyte is very unlikely with the used analyte concentrations (the number of molecules in solution was one order of magnitude higher than the amount needed to saturate the molecules immobilized on the spot).

2. Steric hindrance on the surface due to binding events

The biotin streptavidin model was chosen due to the exceptionally high affinity. However, on a microarray surface, the binding of analyte could cause steric hindrance decreasing the probability of the reaction partners' encounter. This can slow down the binding rate constant by one order of magnitude (Srisa-Art et al., 2008). This leads to a behavior where a limitation of both the diffusion and the binding kinetics affect the rate of reaction. The steric hindrance effect should be minimized by decreasing the density of binding sites (fewer capture molecules / area). Since the spot area is constant then the density of binding sites depends on the concentration of capture molecules printed on the surface. Therefore, the deviation from the model should not be observed in the lower concentrations of biotin on the surface. However, the deviation was observed in all of the spotting concentrations and was not avoided in lower binding sites density.

3. Diffusion in the hydrogel

In 3D-hydrogel immobilization, the capture molecules are not only immobilized on the surface but they are also embedded within the hydrogel network. The accessibility of the probes inside of the gel could also contribute to the deviation from the assumptions made. Due to the high polymer chain concentration in the hydrogel the accessibility of the molecules within the hydrogel will be different from those at the surface and the diffusion coefficient of the analyte in the hydrogel is expected to be lower than in solution. For this reason, the accessibility of the capture molecules within the hydrogel and the ability of the analyte molecule to diffuse through were investigated.

5.3. STUDY OF THE DIFFUSION IN THE HYDROGEL

The diffusion in the hydrogel used for the 3D immobilization is an important aspect that is thought to affect the performance of the microarray. To study this effect, a model where the microarrays were dip-coated with a thin layer of the hydrogel was developed (Figure 5.6). The microarrays were printed, washed and then dip-coated with a polymer solution containing PDMAA-5%MABP-2.5%SSNa in ethanol. The arrays were then cross-linked by UV-exposure (3 J/cm^2, λ = 365 nm). This should form a thin homogenous polymer layer on top of the array with a thickness of around 5 nm (Freidank, 2005) and a mesh size (ξ) of around 11.3 nm (Pandiyarajan, 2013).
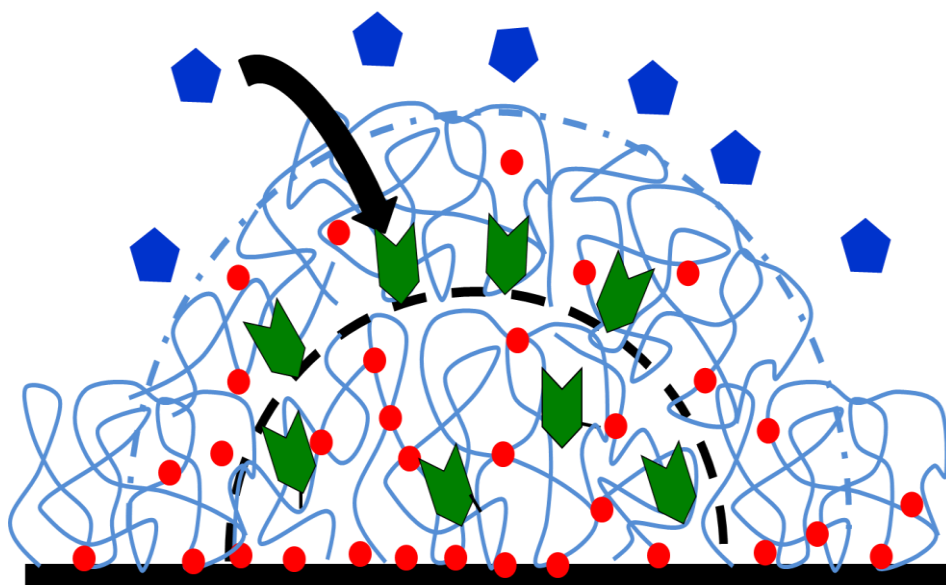
Figure 5.6 Schematic showing a spot of the developed model where the hydrogel coating on the array simulates the diffusion process in the hydrogel (see process number 3 in (Figure 2.1)). The arrow represents the diffusion step through the hydrogel barrier coat which limits the binding of analyte molecules to the spot surface. The blue symbols represent analyte molecules, the green ones the capture molecules, and the red dots are cross-linking points.

The effect of the coating process on the signal of an immobilized fluorophore was studied by measuring the signals of immobilized fluorophores to assess the amount of biological species washed away in such process. The signals of three identical spots on two different arrays were measured directly after printing, after washing and after the coating process. The signal measured directly after printing was considered as reference value (value set to 1). The immobilization efficiency measured for the 3D immobilization technique was 60 %, which is in good agreement with the literature (Rendl et al., 2011; Moschallski et al., 2010; Rubina et al., 2005; Rubina et al., 2003). In case of the coated arrays, a second loss in immobilized biomolecules was observed and the obtained signal was dropped to 30% of the initial value obtained (Figure 5.7).
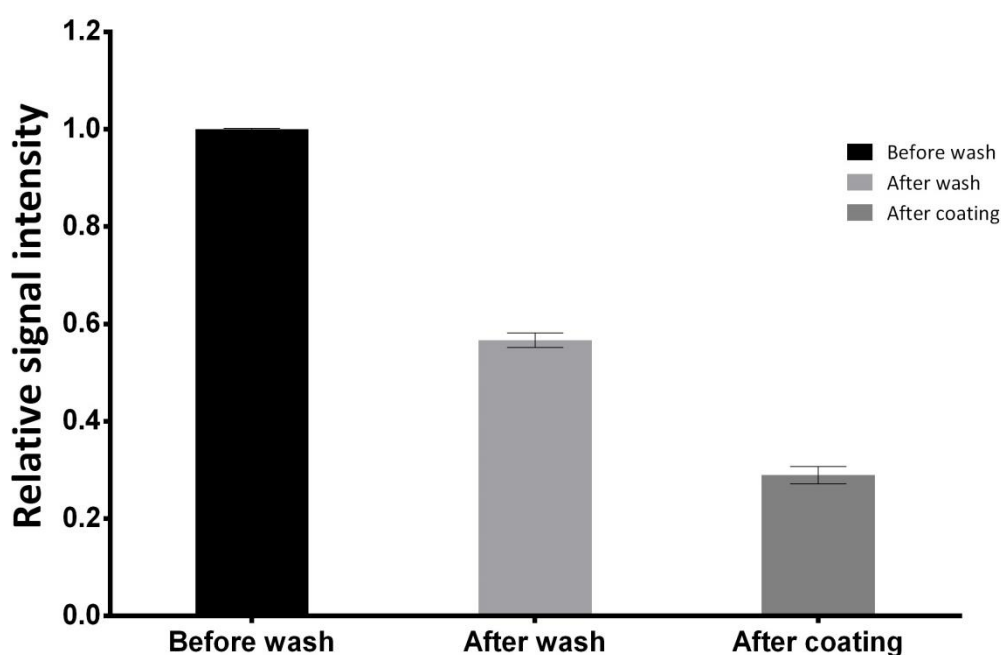
Figure 5.7 The effect of coating on the signal obtained from the microarray spots. The signals correspond to the coupling control immobilized on the array. The relative signal was calculated from the mean value of 2 measured microarrays and the signal directly after print (before washing). The error bars represent the inter- and intra-array standard deviation.

This loss in signal could be attributed to the second UV irradiation, which could have caused photo-bleaching of the fluorophores and/or slight degradation of the polymer network leading to a loss of the biological species.

Therefore, a decrease in the amounts of immobilized species on the microarray due to the coating process is expected. Indeed the observed signals for the microarrays dropped to 30 % of the initial values. Although, there is a loss in the amounts of immobilized biotin, the functionality of the remaining molecules is not affected. For this reason, the highest concentration of biotin oligonucleotides immobilized on the surface (10 μM) was normalized

to its corresponding maximum signal and then used to investigate the effect of the hydrogel on the signal development.

To understand how the hydrogel affects the signal development on a 3D-hydrogel microarray, microarrays coated with PDMMA-5%MABP-2.5%SSNa co-polymer (1 mg/ml) were prepared. The expected layer thickness for this coating concentration is about 5 nm (Freidank, 2005). The arrays were incubated with 1 µg/ml streptavidin-Cy5 and a series of measurements were performed over a period of 3 hours. The obtained data were normalized to the maximum signal obtained after 3 hours shown in (Figure 5.8). The two-compartment model showed very good agreement when fitted to the data (r^2 = 0.935, X^2 = 0.0042). The characteristic mass transport binding time (Tm =0.48 hours) was derived from the fitting.
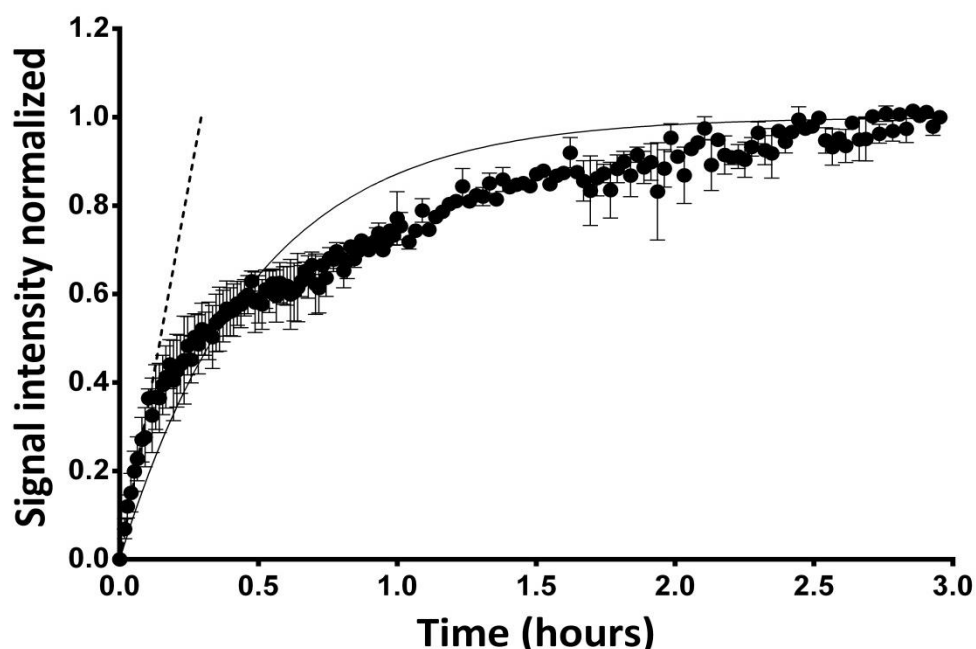
Figure 5.8 Observed kinetics of biotin-streptavidin interaction in the hydrogel coated arrays. The average of 2 microarrays with on chip redundancy of 12 spots is shown. The solid line represents the best fitting according to the two compartment model r^2 = 0.935, X^2 = 0.0042. The dotted line represent the linear regression analysis of the first 10 data points $Y = 3.234X$, r^2 = 0.945. The error bars represent the standard error.

The observed kinetics for the coated and the non-coated microarrays were compared using non-paired two-sided t-test to check the significance of difference. There was no significant difference observed for the signal development (P = 0.062 > 0.05) (Figure 5.9). However, the maximum signal from the coated arrays was lower due to the loss in molecules during the coating process.

This non-significant difference could be caused by the thin polymer layer of about 5 nm in thickness resulting from the dip-coating process (using 1 mg/ml PDMMA-5%MABP-2.5%SSNa co-polymer) (Freidank, 2005). Moreover, the mesh size for the swollen gel is 11.3 nm (Pandiyarajan, 2013). This should not hinder the diffusion of the streptavidin through the network of the hydrogel (hydrodynamic radius = 2.5 nm) (Swift et al., 2006). Another possibility that the resulting layer was very thin and insufficient to cover the spots. For this reason, the layer thickness was varied to ensure a complete coverage of the arrays.
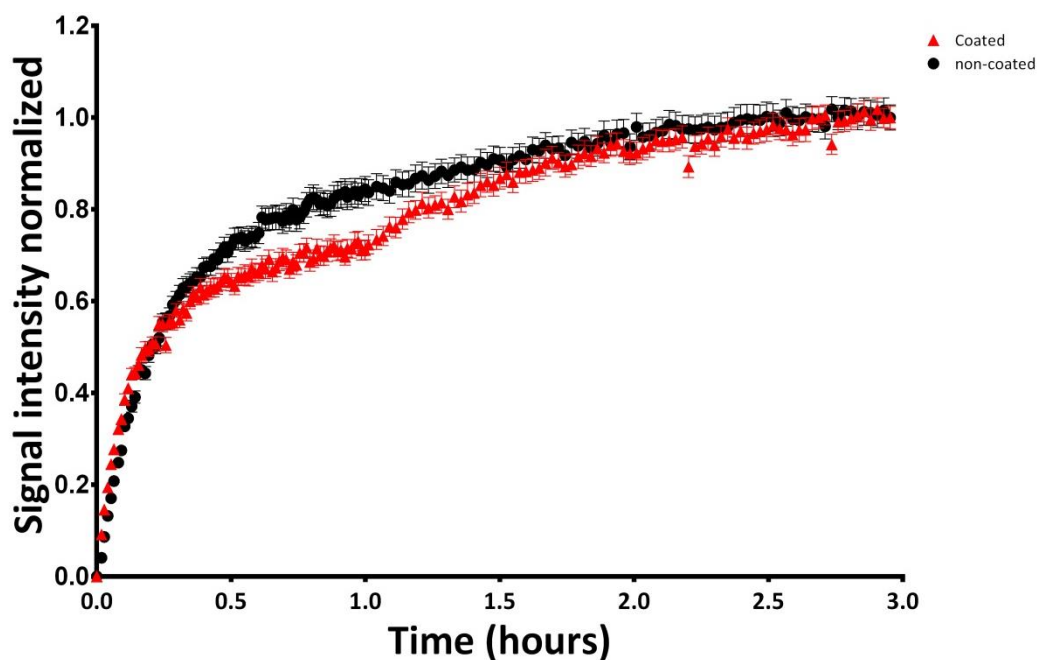
Figure 5.9 Plot comparing the non-coated microarrays assay kinetics to the coated microarrays data from experiments in Figure 5.4 and Figure 5.8. The error bars represent the standard error.

In order to study the effect of the layer thickness on the microarrays kinetics, microarrays were dip coated with higher concentrations (5 mg/ml and 10 mg/ml) of polymer (PDMMA-5%MABP-2.5%SSNa) in the coating solutions. This results in thicker layers (7 and 12 nm respectively) of the deposited polymer on the arrays (Freidank, 2005). These arrays showed no signal during the 3 hours measuring time. However, measuring these arrays after an incubation of 24 hours, a specific binding signal was observed (Figure 5.10). This finding was attributed to the slow and hindered diffusion through the hydrogel layer.
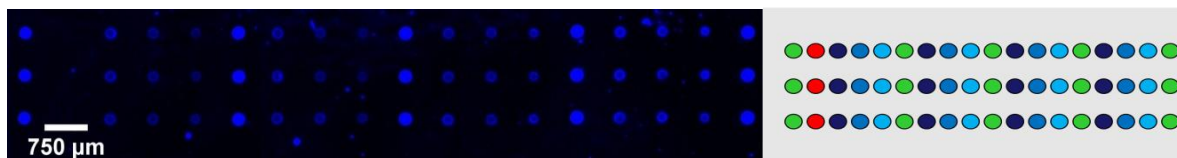
Figure 5.10 False color image of the measured array (coated with 5 mg/ml polymer solution). Specific binding signal was observed. The green spots represent the coupling controls (oligo-Cy5), the red spots are the negative control (polymer without oligonucleotides), and the blue spots represent 10, 5 and 1 µM biotin labeled oligonucleotides. The scale is the inter-spot distance of 750 µm.

The mesh size of the hydrogel is an important parameter that can affect diffusion of the molecules. To assess the effect of the mesh size on the diffusion of proteins in the hydrogel, microarrays coated with PDMMA-1%MABP-2.5%SSNa co-polymer were prepared. This results in a hydrogel in a mesh size (ξ) of 24 nm (Pandiyarajan, 2013). Accordingly, microarrays were dip-coated with polymer solution (1 mg/ml) to produce a thin layer of hydrogel. The arrays were incubated with 1 µg/ml streptavidin-Cy5 and a series of measurements were done in the ATR over a period of 3 hours. The data were normalized to the maximum signal obtained after 3 hours. The assay kinetics was analyzed and the two compartment model was fitted to the data (r^2 = 0.968, χ^2 = 0.002) (Figure 5.11). The characteristic mass transport binding time (Tm =0.33 hours) was derived from the fitting.
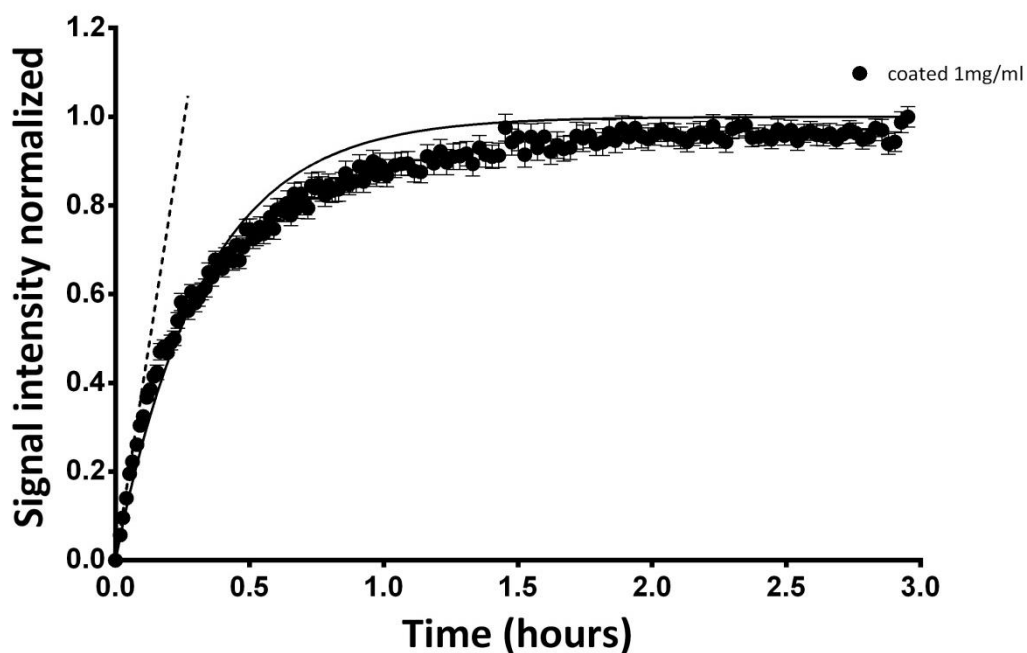
Figure 5.11 Observed kinetics for biotin-streptavidin interaction in microarrays coated with PDMAA-1%MABP-2.5%SSNa co-polymer. The data points represent the average of 2 microarrays with on chip redundancy of 12 spots. The solid line represent the fitting of the two compartment model r^2 = 0.968, X^2 = 0.002 and the dotted line represent the linear regression analysis of the first 10 data points $Y = 3.87X$, r^2 = 0.986. The error bars represent the standard error.

To evaluate the effect of this added layer, the kinetics observed was compared to the kinetics observed for the non-coated microarrays using non-paired two-sided t-test to check for the significance of difference. There was no significant difference observed (P = 0.189 > 0.05) (Figure 5.12). This further confirms that this very thin layer of polymer coating did not affect the diffusion of the proteins.
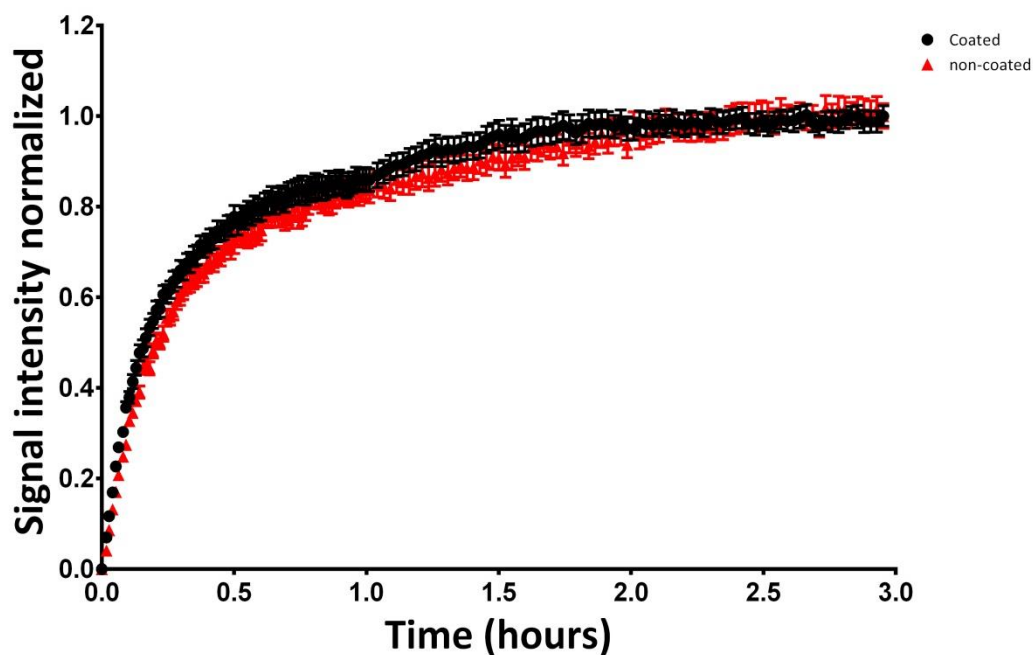
Figure 5.12 Plot comparing the non-coated microarrays assay kinetics to the coated microarrays data from experiments in (Figure 5.4) and (Figure 5.11). The error bars represent the standard error.

To further investigate the diffusion process and simulate a condition where the layer thickness resembles that of the microarray spot (15 $\pm$ 5 nm as measured by (Moschallski, 2007), the microarrays were dip-coated with 5 mg/ml and 10 mg/ml coating solutions (PDMMA-1%MABP-2.5%SSNa). This allows the evaluation of the effect of both the layer thickness and the mesh size.
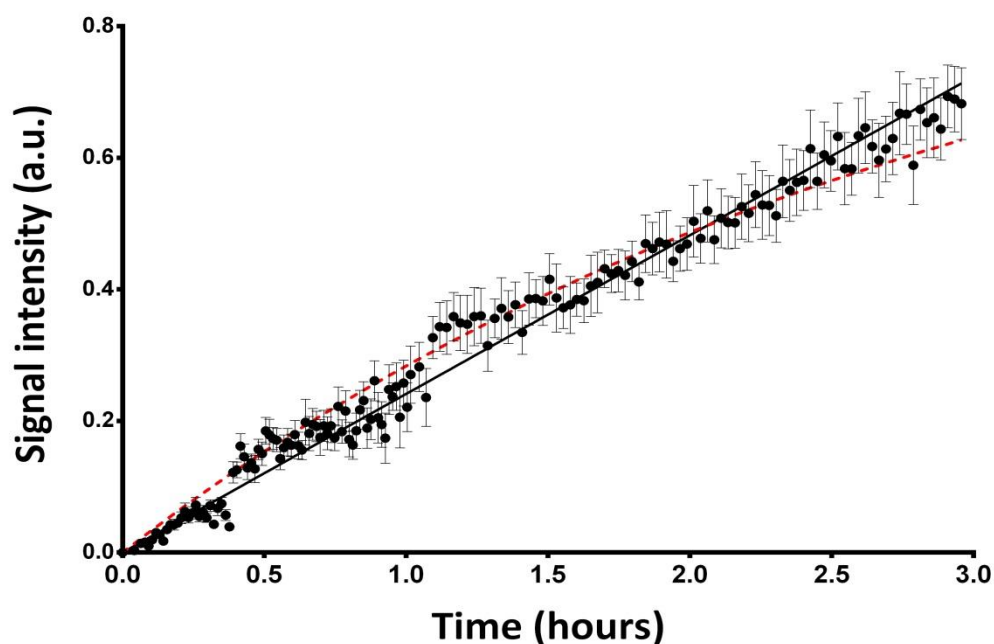
Figure 5.13 The observed kinetics of biotin-streptavidin using microarrays coated with a PDMAA-1%MABP-2.5%SSNa co-polymer solution (5 mg/ml). The data point represents the average of 2 microarrays with on-chip redundancy of 12 spots. The red line represent the two compartment model as fitted to the data $1.8r^2 = 0.984$, $X^2 = 0.000058$ and the solid line is the linear regression analysis $Y = 0.2411X$, $r^2 = 0.982$. The error bars represent the standard error.

In contrast to the results observed in the case of the microarrays coated with PDMMA-5%MABP-2.5%SSNa where the kinetics could not be observed during the 3 hours, here (Figure 5.13) very slow linear development of signal was observed. This linear behavior can be explained by the diffusion of the analyte molecules through the hydrogel layer and the slope reflects the diffusion rate. This linear behavior can be compared to the initial phase of the assay kinetics observed for non-coated microarrays. However, the slope ($Y = 2.82X$) is one order of magnitude higher in the case of non-coated microarrays reflecting faster signals development. Therefore, the two-compartment model was fitted to this data with the maximum signal as obtained from the data shown in (Figure 5.11). The characteristic mass transport time (T_m) was derived from the fitting and was 12.6 hours. However, for the 10 mg/ml no signal was seen in the measuring time of 3 hours. The obtained data were normalized to the maximum signal obtained from the data shown in (Figure 5.11). This allowed comparing the obtained linear behavior kinetics to the exponential kinetics observed in the previous experiment.
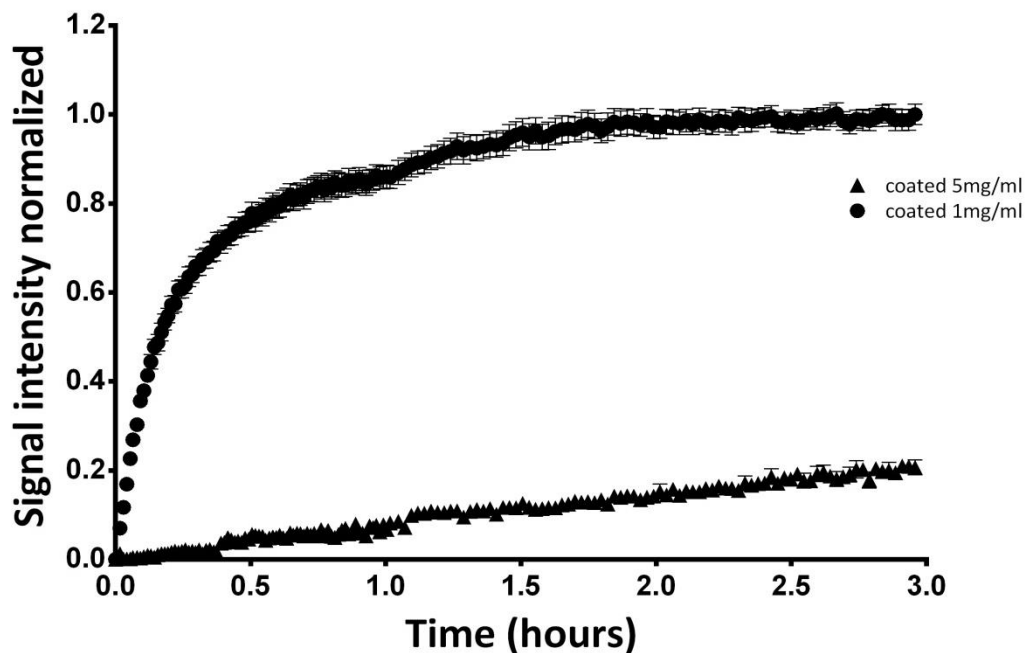
Figure 5.14 The effect of the layer thickness on the rate of signal development. The assay kinetics measured in microarrays coated with thin layer (1 mg/ml) were compared to those from the thick layer (5 mg/ml). A slowdown of the signal development can be seen in the case of the thick layer.

Increasing the hydrogel layer thickness slowed down the initial signal development on the microarrays by a factor of ten (Figure 5.14). This is effect is due to a different diffusion coefficient for the analyte molecules in solution and in hydrogel. The mesh size and layer thickness both can affect the rate of diffusion in the hydrogel. The mesh size will change the diffusion coefficient due to either size exclusion effect or steric hindrance. On the other hand, the thickness will change only the distance the analyte molecules have to travel through the hydrogel. Moreover, the characteristic binding time (T_m) for the microarrays coated with 1 mg/ml was 0.33 hours in comparison with 12.6 hours for the microarrays coated with 5 mg/ml. The obtained assay kinetics proved the ability of the molecules to diffuse through the hydrogel. However, this diffusion could be limited depending on the properties of the analyte molecules and the matrix of the hydrogel.

5.4. A NOVEL MODEL TO DESCRIBE THE BIOCHEMICAL ASSAY KINETICS IN 3D-HYDROGEL MICROARRAYS

Based on the previous results, it was concluded that the linear increase in the signal seen in (Figure 5.13) and the deviation from the two-compartment model could be due to the hindered diffusion in the hydrogel. The linear deviation from the two-compartment model could be explained by the linear kinetics observed for coated microarrays (Figure 5.13).

To confirm this finding, the observed kinetics that showed deviation from the two compartment model was reanalyzed. The phase showing the linear deviation was identified (Figure 5.15). This linear deviation was plotted against the corresponding measuring times separately and analyzed using the linear regression analysis (Figure 5.16). This deviation is linear with a slope reflection the mass transport rate in the hydrogel and an intercept indicating the maximum signal according the two-compartment model.
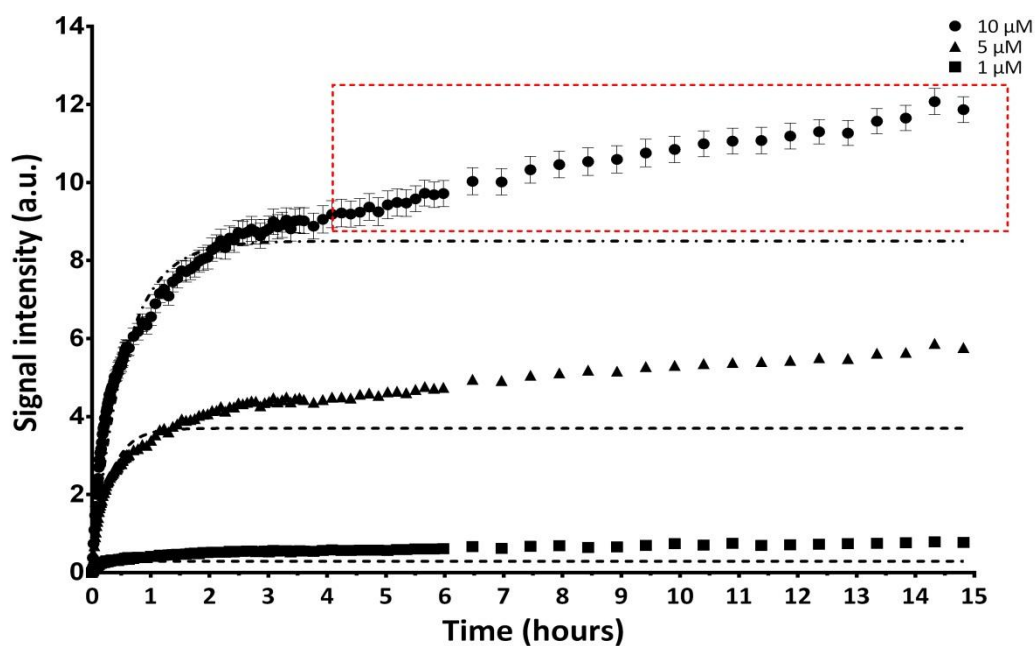
Figure 5.15 Observed kinetics of biotin-streptavidin interaction using 3D-hydrogel microarrays. The red box is inserted to highlight the deviation phase.
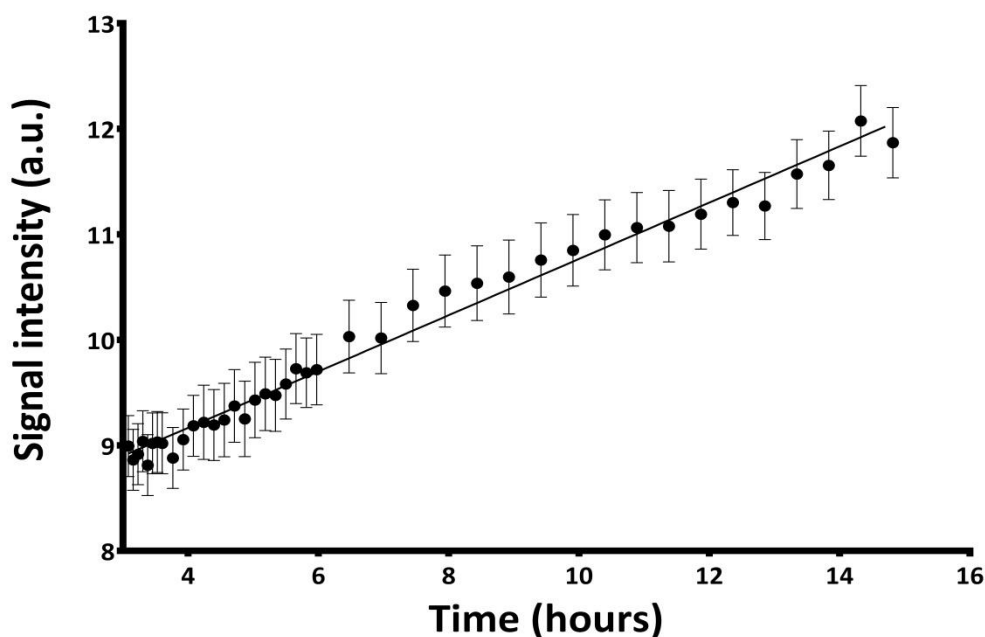
Figure 5.16 Linear regression analysis of the linear deviation observed in the kinetics using 3D-hydrogel microarrays $Y = 0.2667X + 8.1$, $1.8r^2 = 0.984$. The slope reflects the diffusion in the hydrogel and the intercept indicates the maximum signal according to the two-compartment model. The error bars show the standard error.

The data observed in (Figure 5.16) were compared to the observed kinetics for the diffusion in the hydrogel with a linear equation ($Y = 0.2411X$) (Figure 5.13). It can be seen that the two behaviors are identical and that the slope, which represents the mass transport in the hydrogel in both cases, is comparable. Therefore, the two-compartment model can be used to describe only the initial part of the binding process on 3D-hydrogel microarrays. However, this model is insufficient for describing the overall kinetics of the biochemical assay in 3D-hydrogel microarrays. The two-compartment model should be modified to account for the additional diffusion in the hydrogel phase. Such process is seen to be linear and a linear descriptor in the equation could modify the model to account for this phase. However, the process is more complex and this linear descriptor would not be proper since analyte molecules will eventually occupy and deplete the binding sites in the spots. This will lead to a thermodynamic steady state. Therefore, the proper descriptor for this phase would be an exponential component in the equation. Through modifying the two-compartment model single exponential equation by adding an additional exponential component to account for the diffusion in the hydrogel, the following equation was formulated:

$$S(t) = S_{max1}\left(1 - \exp\left(-\frac{t}{\tau_m}\right)\right) + S_\infty\left(1 - \exp\left(-\frac{t}{\tau_{m\,gel}}\right)\right) \qquad 1.31.$$

With

- $S(t)$: The signal developed after specific time t [a.u.]
- S_{max1}: max signal intensity for the first exponential equation [a.u.]
- τ_m: The characteristic binding time of mass transport kinetics [s]
- S_{max2}: The maximum signal at steady state [a.u.]
- $\tau_{m\,gel}$: The characteristic binding of diffusion in the hydrogel kinetics [s]

The developed model was fitted to the data and the parameters mentioned above were derived. The derived parameters from the developed bi-exponential showed good agreement with the parameters derived from the two-compartment model for the initial phase, an overall improvement in the fitting was observed (Table 2). The fitting was evaluated using ($r^2 = 0.992$ $x^2 = 0.06$) for the bi-exponential model and compared to the fitting from the two-compartment model the coefficient of determination approached unity and the reduced chi square approximates to zero which indicates a good fit (Figure 5.17).
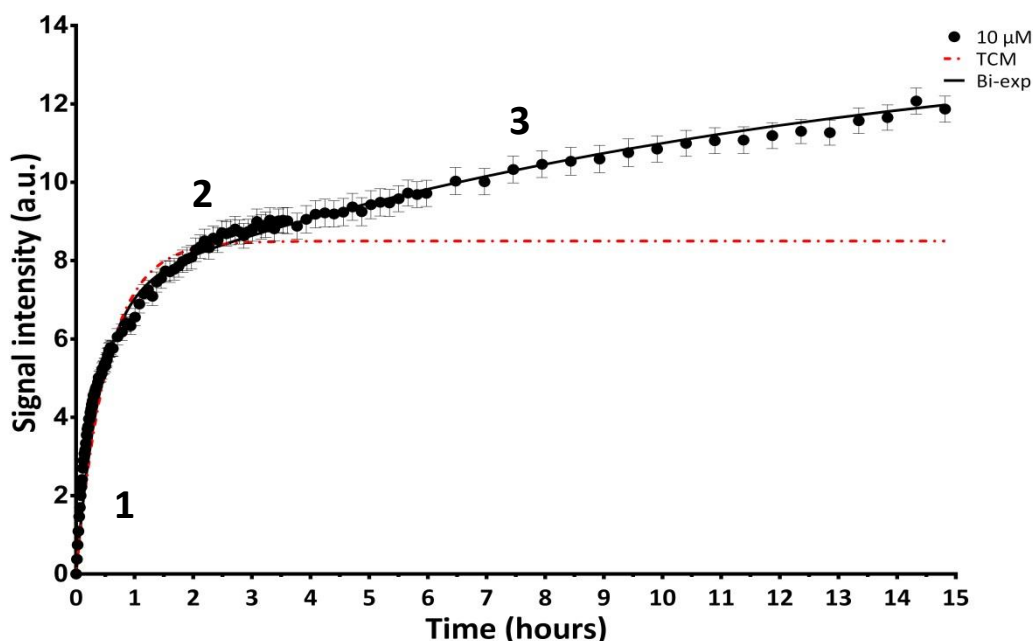
Figure 5.17 Biochemical assay kinetics measured using 3D-hydrogel shown in (Figure 5.3). The black line represents the developed function fitted to the data ($r^2 = 0.992$ $x^2 = 0.06$) and the red line represents the fitting according to two-compartment model ($r^2 = 0.911$ $x^2 = 0.4$). The numbers show the different processes of the binding shown in (Figure 5.18).

Table 2 The parameters obtained from fitting both the two-compartment and the modified two-compartment (bi-exponential) models to the measured kinetics shown in (Figure 5.17).

Parameter	TCM	Bi-exponential model
T_m	0.53	0.436
S_∞	8.1	12.924
T_{mgel}	-	13.244
S_{max1}	-	7.82
S_{max2}	-	5.104

Using the developed model, the diffusion coefficients for streptavidin both in solution and in the hydrogel can be calculated by two methods. The first one by using the obtained mass transport constant times (T_m) and the second using the slope of the linear phases. For this reason, a relation between the signal intensity and the corresponding number of analyte molecules had to be derived (Figure 8.4). The calculated diffusion coefficients found to be in good agreement with the literature(Table 3) (diffusion coefficient for streptavidin = $1.3 \times 10^{-6} cm^2/s$ (Zhang et al., 2007)). The calculations are provided in the appendix.

Table 3 The diffusion coefficients for streptavidin in solution (aqueous buffer) and in the hydrogel as calculated from the (T_m) and the slope of the signal development.

Method of calculation	Diffusion coefficient in solution	Diffusion coefficient in the hydrogel
The slope of the linear phase	$2.99 \times 10^{-6} cm^2/s$	$4.5 \times 10^{-8} cm^2/s$
Using (T_m)	$1.23 \times 10^{-6} cm^2/s$	$4.04 \times 10^{-8} cm^2/s$

The mass transport limited kinetics occurring with the 3D-hydrogel could be described with the developed model. The kinetics can be broken down to 4 separate processes, each can be seen in the kinetic curve (Figure 5.17).

1. The initial linear phase with a slope that reflects the change in analyte concentration and it depends on the mass transport in the solution (Figure 5.18).
2. The second phase is exponential and in this case marks the saturation of the molecules only on or very close to the surface of the spot (Figure 5.18).
3. The third linear phase after the molecules on the surface of the spot are saturated the analyte diffuses in the hydrogel at a mass transport rate proportional to the slope of the linear regression (Figure 5.18).
4. The fourth phase which is an exponential phase that reaches steady state phase due to saturation of the total amount of molecules in the spot (Figure 5.18). This phase was not reached experimentally. The time calculated for the reaction to reach the steady state is about 5 days.
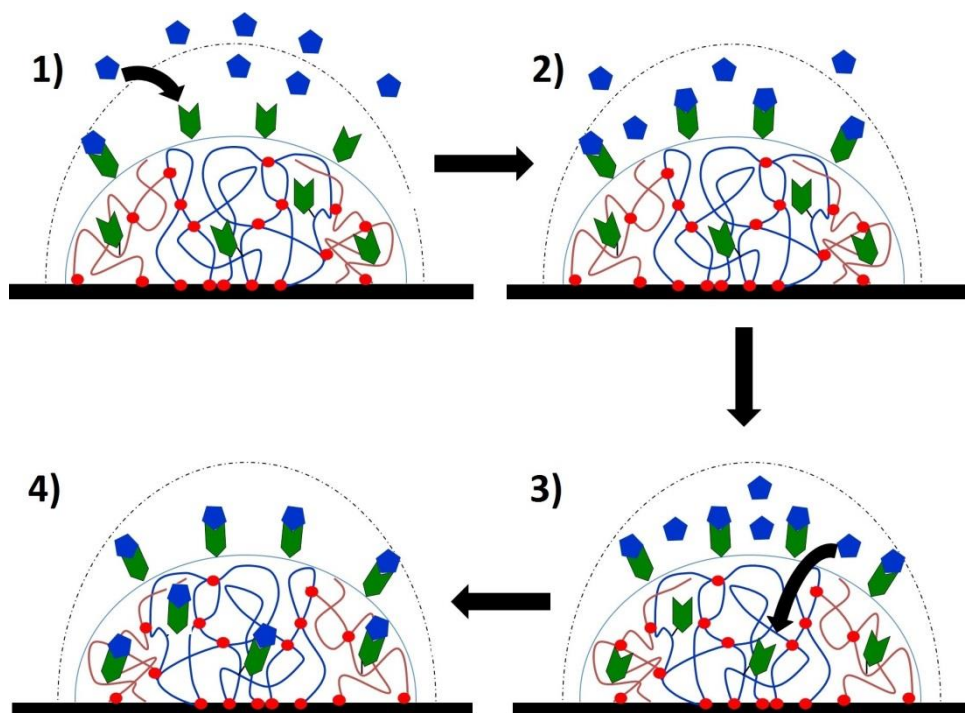
Figure 5.18 The kinetic processes involved in the signal development of 3D-hydrogel microarrays. 1) Represents the initial linear phase reflecting the linear signal development due to mass flux from the solution to the surface of the spot, 2) represents the end of phase one and the pseudo steady state, 3) represents the diffusion in the hydrogel and the linear part reflects the diffusion rate in the hydrogel, and 4) thermodynamic equilibrium due to saturation of the binding sites. The blue symbols represent analyte molecules, green represent capture molecules, and the red dots represent cross-linking points.

5. SUMMARY AND CONCLUSION

The results presented in the experimental work of this thesis addressed the complex assay kinetics performed using the 3D-hydrogel microarrays. First, a microarray to study the assay kinetics using 3D-hydrogel microarrays was designed and the optimum working concentrations were determined. This microarray model allowed the kinetic measurements using an advanced fluorescence detection strategy based on fluorescence in an attenuated total reflection mode. The observed kinetics was compared to the two-compartment model, a model used to describe the mass transport limited assay kinetics in 2D microarray. The observed kinetics showed very good agreement with only the initial phase of the model while at later stages the measured kinetics showed deviations from this model. The reasons for these deviations such as the analyte depletion, steric hindrance and the diffusion in the hydrogel were considered. The used microarray design and the experimental conditions allowed the exclusion of the first two reasons. A hypothesis that the deviation observed is due to an additional diffusion step in the hydrogel was formulated.

To test this hypothesis, a novel microarray model was developed to study the diffusion in the hydrogel. In this model, the microarrays were coated with the same hydrogel used for the 3D immobilization. This allowed studying the diffusion behavior of biomolecules through the hydrogel and its effects on the kinetics. The layer thickness and mesh size were varied to simulate a state where the signal development is controlled only by the diffusion of analyte molecules through the added hydrogel layer. The calculated diffusion coefficient in the hydrogel was two orders of magnitude less than in solution. The diffusion coefficient in solution agrees well with the literature and show the suitability of this simple approach to gain more information about the impact of diffusion. The observed kinetics was compared to the microarrays with no hydrogel coating. The hydrogel layer was found to represent a limitation for the diffusion of the analyte molecules and greatly affected the observed kinetics when its thickness was about 12 nm. The observed kinetics was linear and very slow compared to the non-coated case. These results were comparable to the deviation seen in the first experiments. The signal development behavior in both cases was very slow and linear.

Based on these findings the two-compartment model, which accurately describes the initial kinetics, was modified to describe the complete kinetic processes involved in the signal development of 3D-hydrogel microarrays. This modification was done by including an additional exponential term in the equation to account for the slower signal development caused by the analyte diffusion through the hydrogel in the latter phase of the kinetics. The developed model was fitted to the observed kinetics to test its ability to describe the complete processes involved in 3D-hydrogel biochemical assay kinetics. The model accurately described the complete kinetic processes involved in the signal development on 3D microarrays taking the following conditions into consideration:

1. The number of analyte molecules in solution is higher than that of the capture molecules immobilized on the surface.
2. The used analyte concentration in the biochemical assay is higher than the K_d value.
3. The binding reaction rate is fast compared to the mass-transport (diffusion) rate (i.e. the reaction is diffusion limited).
4. The developed depletion zones are always of height smaller than the height of the incubation chamber due to the excess analyte molecules in solution.
5. The analyte molecules have significantly different diffusion coefficient in the used buffer solution than in the hydrogel matrix.

In conclusion, the understanding of the kinetic processes involved in 3D-hydrogel microarrays is a prerequisite for the design of fast, accurate and highly sensitive diagnostic microarrays. The valuable information gained from these studies about the limitations and their magnitude is a huge step forward to improve the microarray performance parameters (i.e. high sensitivities in short incubation times). The limitation imposed by the diffusion in the hydrogel matrix of 3D-micorarrays goes far beyond the slow signal development. For a typical microarray sandwich immunoassay, the analyte molecules are usually small and can diffuse and bind to the immobilized capture molecules within the hydrogel. However, for the detection step using a detection antibody which is bigger in size than the mesh size of the hydrogel, the size exclusion effect will limit the antibody from diffusing into the gel. This will result in bound analyte molecules that cannot be detected and will compromise the achieved sensitivities by the 3D-hydrogel microarrays.

The developed model is a valuable tool in the process of understanding the complex assay kinetics in 3D hydrogel microarrays and it can be used to estimate the previous mentioned limitation and the accessibility of the molecules.

6. OUTLOOK

Mixing and applying microfluidics in 3D-hydrogel microarrays is a promising solution to overcome the mass transport limitations. However, the application of mixing or convective flow is expected to improve the diffusion of analyte in solution but it will have very limited effect on the improvement of the diffusion of the analyte molecules in the hydrogel. This will lead to very fast initial phase kinetics and then a hindered slow phase due to diffusion in the hydrogel. Therefore, the effect of mixing on the kinetics should be investigated in light of these findings.

The size of both the capture molecule and the analyte would be of crucial importance. Moreover, streptavidin, the analyte used throughout this work, is a relatively small protein (r=2.5 nm) (Swift et al., 2006) and its diffusion was not hindered by size exclusion of the used hydrogel matrix (mesh size = 11.3 nm) (Freidank, 2005). Therefore, the size of the analyte molecules should also be taken into consideration when designing the 3D-hydrogel microarrays. Analytes of sizes larger than the mesh size of the hydrogel matrix will not be able to diffuse through the matrix due to size exclusion effects. This will make the capture molecules immobilized within the hydrogel inaccessible to the analyte affecting the assay sensitivity. This effect should be further investigated and assessed.

This limitation may or may not be overcome in the future, however, an alternative to the typically used end-point measurement could be the dynamic measurements of the initial kinetics for the bio-molecular interaction using 3D hydrogel microarrays. A detection technique based on dynamic measurements combined with a relation between the slope of the initial linear kinetics to the concentration of the analyte would enable fast results in short incubation times. Moreover, this will allow for the clear definition of the measurement point where the signal is detected and will lead to less scattering of the obtained results and eventually higher accuracy.

7. REFERENCES

Abel, L., Kutschki, S., Turewicz, M., Eisenacher, M., Stoutjesdijk, J., Meyer, H.E., Woitalla, D., May, C., 2014. Autoimmune profiling with protein microarrays in clinical applications. Biochimica et Biophysica Acta (BBA) - Proteins and Proteomics 1844, 977-987.

Angenendt, P., 2005. Progress in protein and antibody microarray technology. Drug discovery today 10, 503-511.

Bally, M., Halter, M., Vörös, J., Grandin, H.M., 2006. Optical microarray biosensing techniques. Surface and Interface Analysis 38, 1442-1458.

Bange, A., Halsall, H.B., Heineman, W.R., 2005. Microfluidic immunosensor systems. Biosensors and Bioelectronics 20, 2488-2503.

Berrade, L., Garcia, A.E., Camarero, J.A., 2011. Protein microarrays: novel developments and applications. Pharmaceutical research 28, 1480-1499.

Bönisch, A., 2008. Microarray-basierende Untersuchungen zur Kinetik von Biomolekül-Interaktionen, Department of Microsystems Engineering. University of Freiburg, Germany, p. 101.

Brown, A.M., 2001. A step-by-step guide to non-linear regression analysis of experimental data using a Microsoft Excel spreadsheet. Computer Methods and Programs in Biomedicine 65, 191-200.

Buchegger, P., Preininger, C., 2014. Four assay designs and on-chip calibration: gadgets for a sepsis protein array. Analytical chemistry 86, 3174-3180.

Buchegger, P., Sauer, U., Toth-Szekely, H., Preininger, C., 2012. Miniaturized protein microarray with internal calibration as point-of-care device for diagnosis of neonatal sepsis. Sensors 12, 1494-1508.

Buenger, D., Topuz, F., Groll, J., 2012. Hydrogels in sensing applications. Progress in Polymer Science 37, 1678-1719.

Cahill, D.J., 2001. Protein and antibody arrays and their medical applications. Journal of Immunological Methods 250, 81-91.

Diamandis, E.P., Christopoulos, T.K., 1991. The biotin-(strept)avidin system: principles and applications in biotechnology. Clinical Chemistry 37, 625-636.

Ekins, R., Chu, F., Biggart, E., 1989. Development of microspot multi-analyte ratiometric immunoassay using dual fluorescent-labelled antibodies. Analytica Chimica Acta 227, 73-96.

Fick, A., 1855. V. On liquid diffusion. Philosophical Magazine Series 4 10, 30-39.

Fick, A., 1995. On liquid diffusion. Journal of Membrane Science 100, 33-38.

Freidank, T., 2005. Oberflächengebundene funktionelle Polymernetzwerke als Matrix für Nukleinsäure-Microarrays, Department of Microsystems Engineering. University of Freiburg, Germany, Freiburg, p. 303.

Gauthier, M.A., Luo, J., Calvet, D., Ni, C., Zhu, X.X., Garon, M., Buschmann, M.D., 2004. Degree of crosslinking and mechanical properties of crosslinked poly(vinyl alcohol) beads for use in solid-phase organic synthesis. Polymer 45, 8201-8210.

Glökler, J., Angenendt, P., 2003. Protein and antibody microarray technology. Journal of Chromatography B 797, 229-240.

Gonzalez-Gonzalez, M., Jara-Acevedo, R., Matarraz, S., Jara-Acevedo, M., Paradinas, S., Sayagues, J.M., Orfao, A., Fuentes, M., 2012. Nanotechniques in proteomics: protein microarrays and novel detection platforms. European journal of pharmaceutical sciences : official journal of the European Federation for Pharmaceutical Sciences 45, 499-506.

Hall, D.A., Ptacek, J., Snyder, M., 2007. Protein microarray technology. Mechanisms of Ageing and Development 128, 161-167.

Harrick, N.J., 1960. Study of Physics and Chemistry of Surfaces from Frustrated Total Internal Reflections. Physical Review Letters 4, 224-226.

Harris, L.J., Skaletsky, E., McPherson, A., 1998. Crystallographic structure of an intact IgG1 monoclonal antibody. Journal of Molecular Biology 275, 861-872.

Hennion, M.-C., Barcelo, D., 1998. Strengths and limitations of immunoassays for effective and efficient use for pesticide analysis in water samples: A review. Analytica Chimica Acta 362, 3-34.

Iweala, O.I., 2004. HIV diagnostic tests: An overview. Contraception 70, 141-147.

Janeway, C., 2005. Immunobiology : the immune system in health and disease, 6th ed. Garland Science, New York.

Jonkheijm, P., Weinrich, D., Schröder, H., Niemeyer, C.M., Waldmann, H., 2008. Chemical Strategies for Generating Protein Biochips. Angewandte Chemie International Edition 47, 9618-9647.

Joos, T.O., Schrenk, M., Hopfl, P., Kroger, K., Chowdhury, U., Stoll, D., Schorner, D., Durr, M., Herick, K., Rupp, S., Sohn, K., Hammerle, H., 2000. A microarray enzyme-linked immunosorbent assay for autoimmune diagnostics. Electrophoresis 21, 2641-2650.

Killard, A.J., Deasy, B., O'Kennedy, R., Smyth, M.R., 1995. Antibodies: production, functions and applications in biosensors. TrAC Trends in Analytical Chemistry 14, 257-266.

Klenin, K.V., Kusnezow, W., Langowski, J., 2005. Kinetics of protein binding in solid-phase immunoassays: theory. The Journal of chemical physics 122, 214715.

Kusnezow, W., Syagailo, Y.V., Goychuk, I., Hoheisel, J.D., Wild, D.G., 2006a. Antibody microarrays: the crucial impact of mass transport on assay kinetics and sensitivity. Expert Review of Molecular Diagnostics 6, 111-124.

Kusnezow, W., Syagailo, Y.V., Ruffer, S., Baudenstiel, N., Gauer, C., Hoheisel, J.D., Wild, D., Goychuk, I., 2006b. Optimal design of microarray immunoassays to compensate for kinetic limitations: theory and experiment. Mol Cell Proteomics 5, 1681-1696.

Kusnezow, W., Syagailo, Y.V., Rüffer, S., Klenin, K., Sebald, W., Hoheisel, J.D., Gauer, C., Goychuk, I., 2006c. Kinetics of antigen binding to antibody microspots: Strong limitation by mass transport to the surface. PROTEOMICS 6, 794-803.

Lehr, H.P., Reimann, M., Brandenburg, A., Sulz, G., Klapproth, H., 2003. Real-Time Detection of Nucleic Acid Interactions by Total Internal Reflection Fluorescence. Analytical Chemistry 75, 2414-2420.

Lin, C.C., Metters, A.T., 2006. Hydrogels in controlled release formulations: network design and mathematical modeling. Advanced drug delivery reviews 58, 1379-1408.

Marco, M.-P., Gee, S., Hammock, B.D., 1995. Immunochemical techniques for environmental analysis I. Immunosensors. TrAC Trends in Analytical Chemistry 14, 341-350.

Minton, A.P., 2001. The influence of macromolecular crowding and macromolecular confinement on biochemical reactions in physiological media. J Biol Chem 276, 10577-10580.

Moschallski, M., 2007. 3D-Protein Chips Based on Microstructured Surface-Attached Polymer Networks, Department of Microsystems Engineering. University of Freiburg, Germany, p. 103.

Moschallski, M., Baader, J., Prucker, O., Rühe, J., 2010. Printed protein microarrays on unmodified plastic substrates. Analytica Chimica Acta 671, 92-98.

Moschallski, M., Evers, A., Brandstetter, T., Ruhe, J., 2013. Sensitivity of microarray based immunoassays using surface-attached hydrogels. Anal Chim Acta 781, 72-79.

Neumann, T., 2006. Wiederverwendbare 3D-Polymer-DNA-Chips zur Echtzeitanalyse und kompartimentierten Paralleldiagnostik, Department of Microsystem Engineering. University of Freiburg, Germany, Freiburg, p. 287.

Nicodemus, G.D., Bryant, S.J., 2008. Cell encapsulation in biodegradable hydrogels for tissue engineering applications. Tissue Eng Part B Rev 14, 149-165.

Pandiyarajan, C.K., 2013. The interaction of blood proteins and platelets on surface-attached poly (alkylacrylamide) networks, Department of Microsystems Engineering. University of Freiburg, Germany, Freiburg, p. 210.

Pavlickova, P., Schneider, E.M., Hug, H., 2004. Advances in recombinant antibody microarrays. Clinica Chimica Acta 343, 17-35.

Peoples, M.C., Karnes, H.T., 2008. Microfluidic immunoaffinity separations for bioanalysis. J Chromatogr B Analyt Technol Biomed Life Sci 866, 14-25.

Peppas, N.A., Huang, Y., Torres-Lugo, M., Ward, J.H., Zhang, J., 2000. PHYSICOCHEMICAL FOUNDATIONS AND STRUCTURAL DESIGN OF HYDROGELS IN MEDICINE AND BIOLOGY. Annual Review of Biomedical Engineering 2, 9-29.

Radom, F., Jurek, P.M., Mazurek, M.P., Otlewski, J., Jeleń, F., 2013. Aptamers: Molecules of great potential. Biotechnology Advances 31, 1260-1274.

Ramachandran, N., Larson, D.N., Stark, P.R.H., Hainsworth, E., LaBaer, J., 2005. Emerging tools for real-time label-free detection of interactions on functional protein microarrays. FEBS Journal 272, 5412-5425.

Ray, S., Mehta, G., Srivastava, S., 2010. Label-free detection techniques for protein microarrays: prospects, merits and challenges. PROTEOMICS 10, 731-748.

Rendl, M., 2009. TOWARDS A NOVEL DYNAMIC BIOCHIP PLATFORM FOR REAL-TIME DETECTION AND QUANTIFICATION OF PROTEINS, Department of Microsystems Technology IMTEK. University of Freiburg, Germany, p. 108.

Rendl, M., Bönisch, A., Mader, A., Schuh, K., Prucker, O., Brandstetter, T., Rühe, J.r., 2011. Simple One-Step Process for Immobilization of Biomolecules on Polymer Substrates Based on Surface-Attached Polymer Networks. Langmuir 27, 6116-6123.

Romanov, V., Davidoff, S.N., Miles, A.R., Grainger, D.W., Gale, B.K., Brooks, B.D., 2014. A critical comparison of protein microarray fabrication technologies. The Analyst 139, 1303-1326.

Rubina, A.Y., Dementieva, E.I., Stomakhin, A.A., Darii, E.L., Pan'kov, S.V., Barsky, V.E., Ivanov, S.M., Konovalova, E.V., Mirzabekov, A.D., 2003. Hydrogel-based protein microchips: manufacturing, properties, and applications. Biotechniques 34, 1008-1014, 1016-1020, 1022.

Rubina, A.Y., Dyukova, V.I., Dementieva, E.I., Stomakhin, A.A., Nesmeyanov, V.A., Grishin, E.V., Zasedatelev, A.S., 2005. Quantitative immunoassay of biotoxins on hydrogel-based protein microchips. Anal Biochem 340, 317-329.

Rusmini, F., Zhong, Z., Feijen, J., 2007. Protein immobilization strategies for protein biochips. Biomacromolecules 8, 1775-1789.

REFERENCES

Sauer, U., Domnanich, P., Preininger, C., 2011. Protein chip for the parallel quantification of high and low abundant biomarkers for sepsis. Anal Biochem 419, 46-52.

Schrodinger, LLC, 2010. The PyMOL Molecular Graphics System, Version 1.3r1.

Schunk, P.R., Hurd, A., Brinker, C.J., 1997. Free-Meniscus Coating Processes, in: Kistler, S., Schweizer, P. (Eds.), Liquid Film Coating. Springer Netherlands, pp. 673-708.

Self, C.H., Cook, D.B., 1996. Advances in immunoassay technology. Current Opinion in Biotechnology 7, 60-65.

Sreekumar, A., Nyati, M.K., Varambally, S., Barrette, T.R., Ghosh, D., Lawrence, T.S., Chinnaiyan, A.M., 2001. Profiling of cancer cells using protein microarrays: discovery of novel radiation-regulated proteins. Cancer Res 61, 7585-7593.

Srisa-Art, M., Dyson, E.C., deMello, A.J., Edel, J.B., 2008. Monitoring of Real-Time Streptavidin–Biotin Binding Kinetics Using Droplet Microfluidics. Analytical Chemistry 80, 7063-7067.

Sun, H., Chen, Grace Y.J., Yao, Shao Q., 2013. Recent Advances in Microarray Technologies for Proteomics. Chemistry & Biology 20, 685-699.

Swift, J.L., Heuff, R., Cramb, D.T., 2006. A Two-Photon Excitation Fluorescence Cross-Correlation Assay for a Model Ligand-Receptor Binding System Using Quantum Dots. Biophysical Journal 90, 1396-1410.

Tisone, T.C., Eickhoff, H., 2013. Systems and methods for high speed array printing and hybridization. Google Patents.

Toh, S.Y., Citartan, M., Gopinath, S.C.B., Tang, T.-H., 2015. Aptamers as a replacement for antibodies in enzyme-linked immunosorbent assay. Biosensors and Bioelectronics 64, 392-403.

Toomey, R., Freidank, D., Rühe, J., 2004. Swelling Behavior of Thin, Surface-Attached Polymer Networks. Macromolecules 37, 882-887.

Vitzthum, F., Behrens, F., Anderson, N.L., Shaw, J.H., 2005. Proteomics: From Basic Research to Diagnostic Application. A Review of Requirements & Needs†. Journal of Proteome Research 4, 1086-1097.

Xu, Y., Yang, X., Wang, E., 2010. Review: Aptamers in microfluidic chips. Anal Chim Acta 683, 12-20.

Yager, P., Edwards, T., Fu, E., Helton, K., Nelson, K., Tam, M.R., Weigl, B.H., 2006. Microfluidic diagnostic technologies for global public health. Nature 442, 412-418.

Yimsiri, P., Mackley, M.R., 2006. Spin and dip coating of light-emitting polymer solutions: Matching experiment with modelling. Chemical Engineering Science 61, 3496-3505.

Zhang, L., Dammann, K., Bae, S.C., Granick, S., 2007. Ligand-receptor binding on nanoparticle-stabilized liposome surfaces. Soft Matter 3, 551-553.

Zhu, H., Snyder, M., 2003. Protein chip technology. Current opinion in chemical biology 7, 55-63.

Zubtsov, D.A., Savvateeva, E.N., Rubina, A.Y., Pan'kov, S.V., Konovalova, E.V., Moiseeva, O.V., Chechetkin, V.R., Zasedatelev, A.S., 2007. Comparison of surface and hydrogel-based protein microchips. Anal Biochem 368, 205-213.

8. APPENDIX

Figure 8.1 The obtained signal intensities for the microarrays incubated with 0.5 nM different exposure times (10, 20, and 30 seconds). Plotted the number of fluorophores/μm^2 for the used concentration range (2.7, 0.27, 0.027, 0.0027, 0.00027 and 0.000027). The insert shows limit of detection (LOD) corresponds to approximately 1000 fluorophores/μm^2. The error bars represent the standard deviation.

Figure 8.2 The obtained signal intensities for the microarrays incubated with 5 nM different exposure times (10, 20, and 30 seconds). Plotted the number of fluorophores/μm^2 for the used concentration range (2.7, 0.27, 0.027, 0.0027, 0.00027 and 0.000027). The insert shows limit of detection (LOD) corresponds to approximately 1000 fluorophores/μm^2. The error represent are the standard deviation.
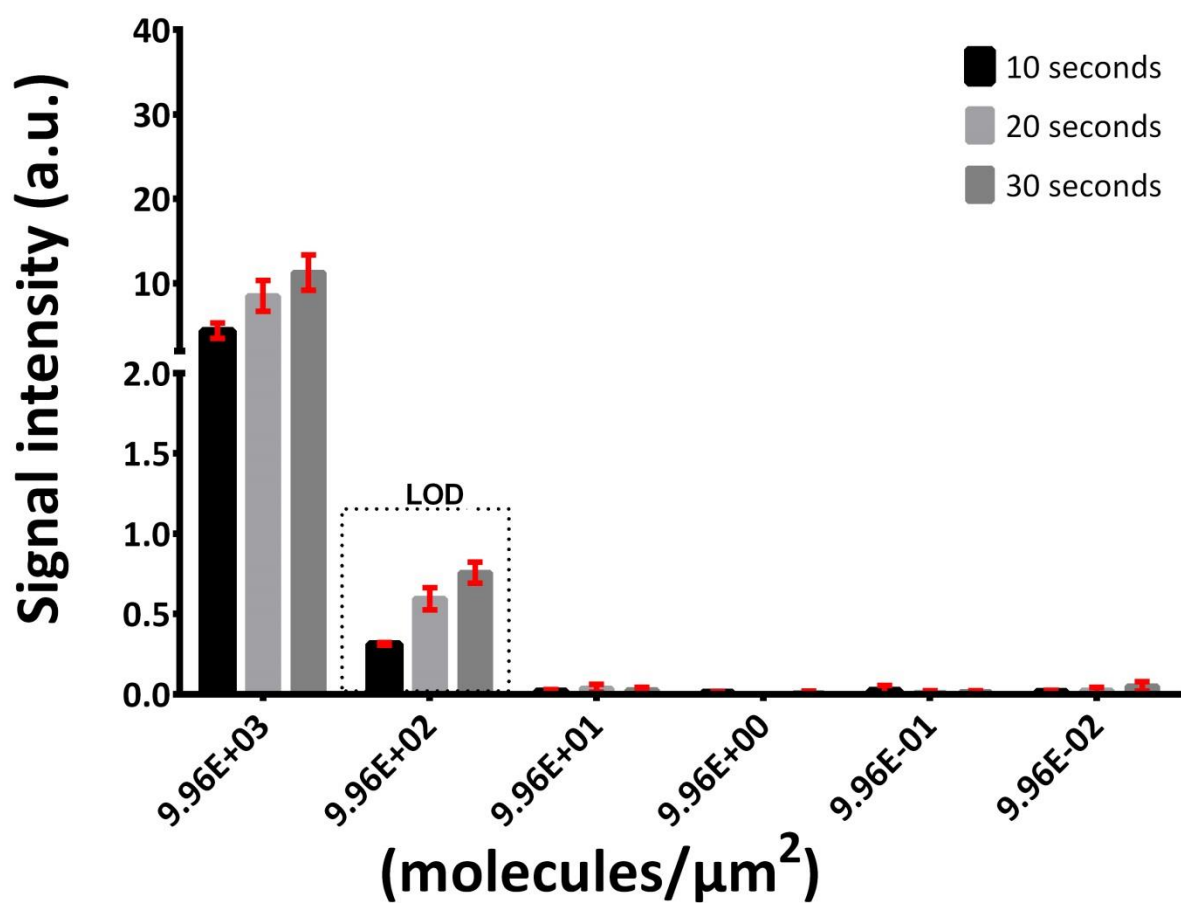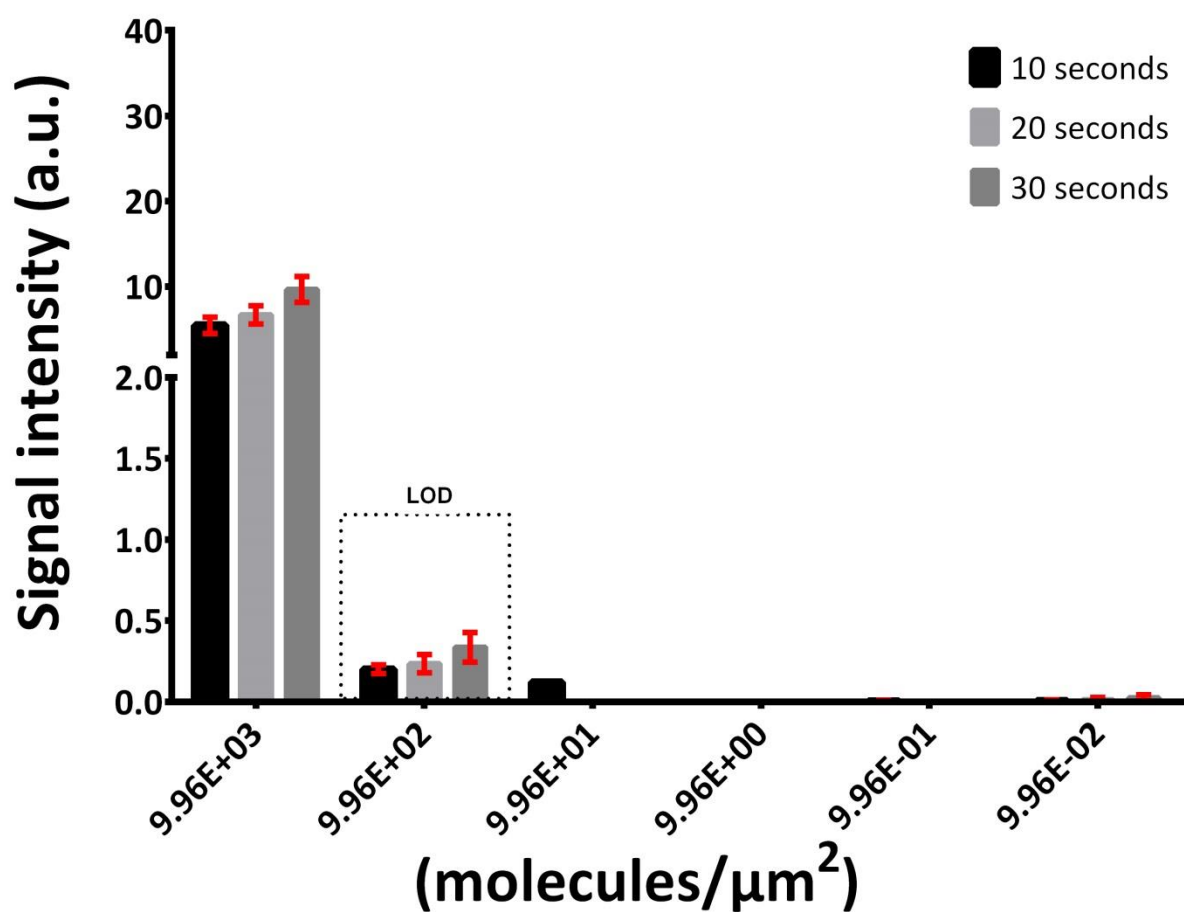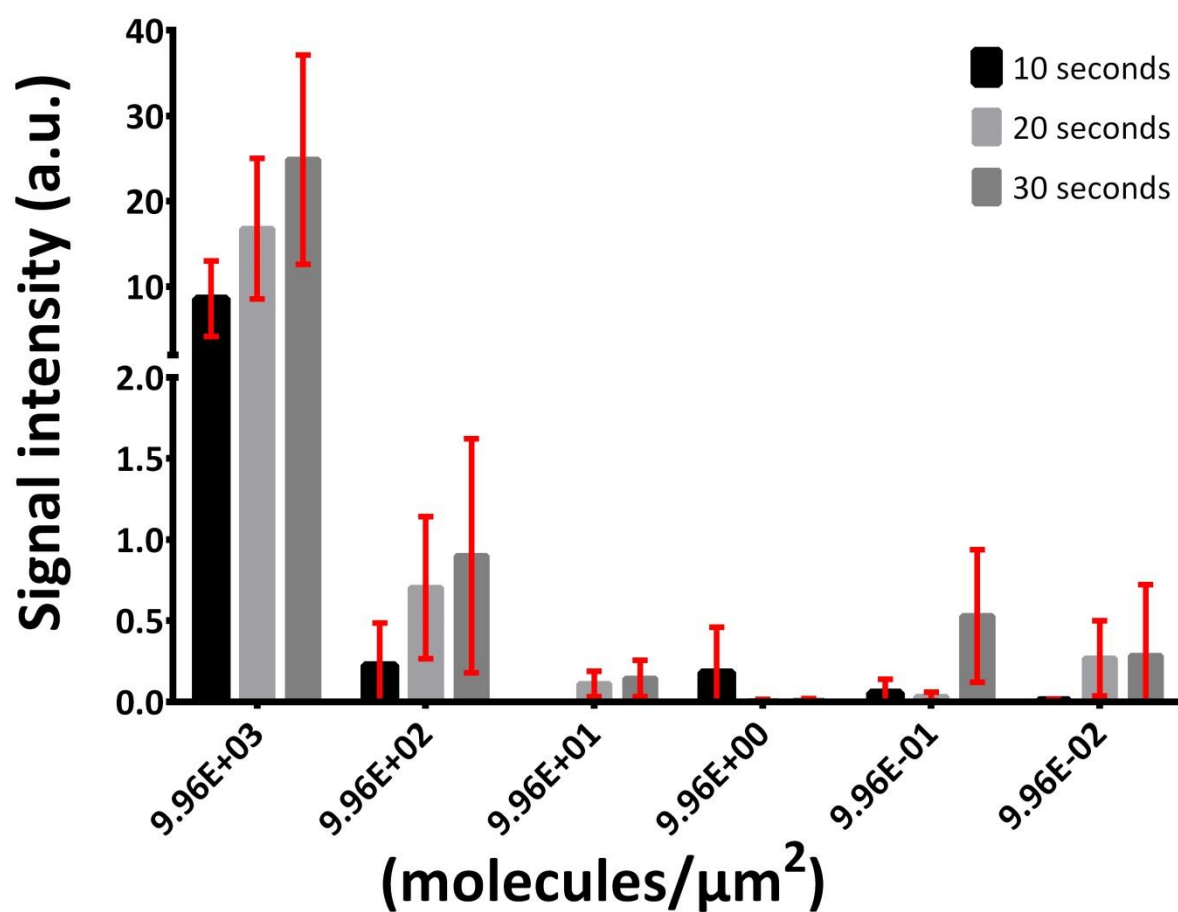
Figure 8.3 The obtained signal intensities for the microarrays incubated with 50 nM different exposure times (10, 20, and 30 seconds). Plotted the number of fluorophores/μm^2 for the used concentration range (2.7, 0.27, 0.027, 0.0027, 0.00027 and 0.000027). The error bars represent the standard deviation.
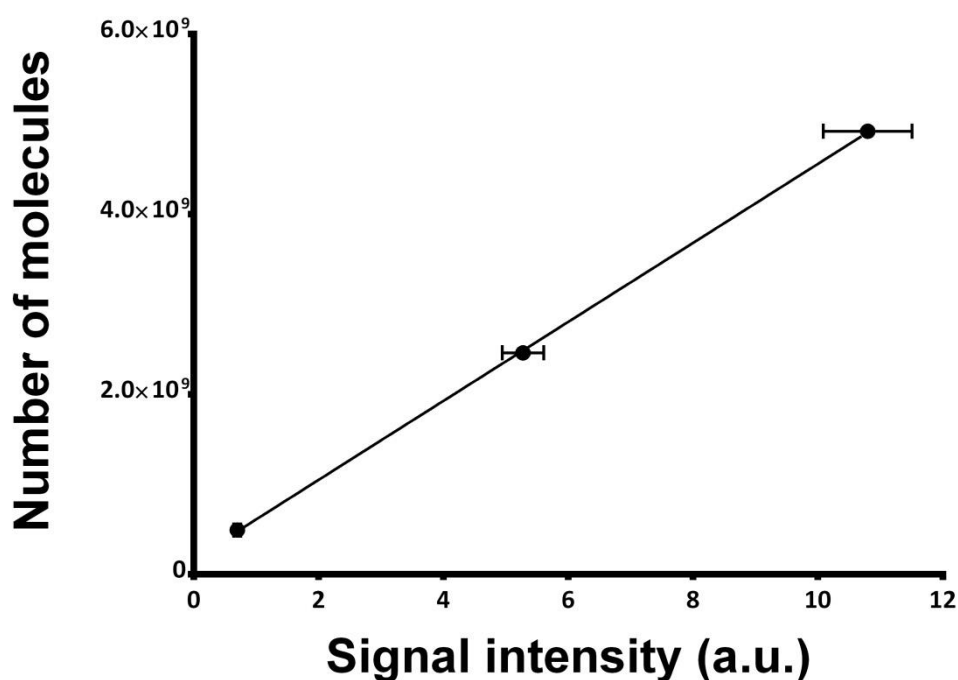
Figure 8.4 Plotted showing the maximum signal obtained from (Figure 5.3) against the maximum number of biotin molecules on the surface of the spot assuming one to one binding interaction the slope of the linear regression gives the number of molecules/signal units. $Y = 4.386 \times 10^8 x + 1.7 \times 10^8, r^2 = 0.99$. The error bars represent the standard deviation.

Figure 8.5 The slope of initial signal development for data shown in Figure 5.17. $Y = 23.08x + 0.11, r^2 = 0.99$. The error bars represent the standard error.

8.1. THE MATHEMATICAL CALCULATIONS FOR THE DIFFUSION COEFFICIENTS

1) using the slope of the linear phase:

The slope from the linear regression for the hydrogel (Figure 5.16):

$$\text{slope} = 0.266 \text{ s. u./hr} = 7.38 \times 10^{-5} \text{ s. u./s} = 3.24 \times 10^{4} \text{molecules/s}$$

The slope from the initial linear signal development (Figure 8.5):

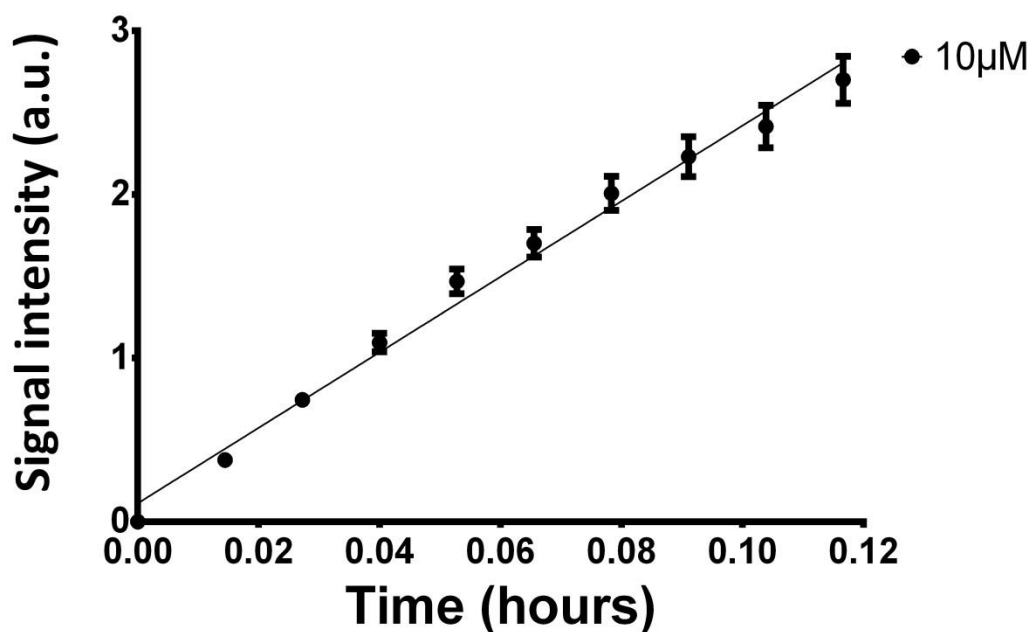$$\text{slope} = 23.08 \text{ s. u./hr} = 6.39 \times 10^{-3} \text{ s. u./s} = 2.8 \times 10^{6} \text{molecules/s}$$

Using Avogadro's number $6.02 \times 10^{23} \text{molecules/mol}$

$$\text{slope for hydrogel} = 5.388 \times 10^{-20} \text{mol/s}$$

$$\text{slope for solution} = 4.65 \times 10^{-18} \text{ mol/s}$$

Area of spot (area of hemisphere), spot radius = 0.01 cm

$$A = 2\pi r^2 = 6.28 \times 10^{-4} \text{ cm}^2$$

Therefore the flux (J) for the hydrogel and for the solution is

$$\frac{\delta c}{\delta a} = 8.57 \times 10^{-17} \text{ mol/cm}^2\text{s}$$

$$\frac{\delta c}{\delta a} = 7.41 \times 10^{-15} \text{ mol/cm}^2\text{s}$$

The initial analyte concentration in the incubation solution is:

$$L_o = 19 \text{ nM} = 19 \times 10^{-12} \text{ mol/cm}^3$$

And the maximum distance travelled by the molecules = spot radius = 0.01

$$\frac{\delta c}{\delta x} = 1.9 \times 10^{-9} \text{ mol/cm}^4$$

From the flux and the change in the distance per time, one can calculate the diffusion coefficient

$$D_{gel} = J \times \frac{\delta x}{\delta c} = 4.5 \times 10^{-8} \text{ cm}^2\text{/s}$$

$$D = J \times \frac{\delta x}{\delta c} = 3.9 \times 10^{-6} \text{ cm}^2\text{/s}$$

2) Using the obtained (T_m) value

From equation 1.10

$$\tau_m = \frac{\pi\rho R}{4DK_d}$$

R = 0.01 cm

ρ = 1.47×10^9 molecules/ cm^2 = 2.44×10^{-15} mol/cm^2

$K_d = 10^{-14}\ M$

The mass transport constant time in hydrogel $\tau_m = 13.244\ hours = 47678.4\ s$

The mass transport constant time in solution $\tau_m = 0.436\ hours = 1569.6\ s$

Therefore the diffusion coefficient in the hydrogel

$$D = \frac{\pi\rho R}{4\tau_m K_d} = 4.04 \times 10^{-8}\ cm^2/s$$

Therefore the diffusion coefficient in the hydrogel

$$D = \frac{\pi\rho R}{4\tau_m K_d} = 1.23 \times 10^{-6}\ cm^2/s$$

8.2.   LIST OF EQUIPMENT

Equipment	Specifications	Supplier
Centrifuges	Centrifuge 5415D	Eppendorf, Hamburg, Germany
	Centrifuge 5804R	Eppendorf, Hamburg, Germany
Mixers	Vortex Genie 1	Scientific Industries, N.Y., USA
	Vortex Genie 2	Scientific Industries, N.Y., USA
Balance	Sartorius CP225D	Sartorius AG, Göttingen, Germany
Ultrasonic Bath	SONOREX RK100H	Bandelin electronic, Berlin, Germany
UV-Crosslinkers	Stratalinker 2400	Stratagene, Ca, USA
Microarrayer	Sciflexarrayer S3	Scienion AG, Berlin, Germany
Microrray reader	ATR 3 (laser light source)	IMTEK, Fraunhofer IPM
Imaging Softwares	Signalyse (2.0.9 US Build 1)	Holger Klapproth Life Science
	Image J (1.46r)	National Institutes of Health, USA
	PyMOL (Version 1.3r1)	Schrödinger, Inc.

8.3.   LIST OF CHEMICALS

Compound	Supplier
PBS (1x)	Sigma, St. Louis, MO, USA
Tween® 20 (Polyoxyethylene (20) sorbitan monolaurate)	Sigma, St. Louis, MO, USA
NaPi (sodium phosphate buffer)	Mixture of disodium hydrogen phosphate (Na_2HPO_4) and sodium dihydrogen phosphate (NaH_2PO_4) with pH 7.0
Nuclease free water	Qiagen, Germany
PDMMA-5% MABP-2.5% SSNa	CPI, IMTEK, University of Freiburg
PDMMA-1% MABP-2.5% SSNa	CPI, IMTEK, University of Freiburg

ACKNOWLEDGEMENTS

I would like to express my sincere gratitude for all those who made it possible for me to complete this thesis. Throughout the time course of this work, many people inspired me and genuinely changed my perspective on the scientific research approach. I would like to express my deepest appreciation and thank all of the persons who stood by my side:

- My thesis supervisor Prof. Dr. Jürgen Rühe for providing the opportunity to work on this very interesting project, for his guidance throughout this work and the great advantage of pursuing my own ideas with many helpful discussions and suggestions.

- Dr. Thomas Brandstetter "Toto" for pointing out the right direction and approach on solving the problems commonly faced in my everyday scientific life. He successfully managed to provide the perfect atmosphere for a stress free work environment. Toto promised me new experiences and he did not fail to deliver. He definitely changed my approach to life by making it clear that a stressed person is unable to answer the simplest questions raised. It was a pleasure to work in his group.

- Prof. Dr. Marta Mollerach for her co-supervision during my thesis and for proofreading this work. She exerted great efforts in solving the bureaucratic administrative issues that could have jeopardized the fulfillment of this program.

- Marc Zinggeler for being a great friend and for his wonderful support during my stay in Freiburg. I would like to thank him for all the fruitful discussions on all aspects of life and the suggestions that contributed significantly to this work. I also would like to thank him for the timely efforts in correcting my thesis and his helpful comments and suggestions.

- Jan Niklas Schönberg for sharing his ideas and for the very interesting discussions that introduced me to the German culture and helped me a lot to integrate with the community. I also thank him for the efforts made to read this thesis and his suggestions and feedback.

- Frau. Anne Buderer and Dr. Andreas Mader for their efforts in introducing me to the microarrays technology and the many important discussions.

- Alexander Dietz for all the shared moments and laughs. I would like to also thank him for being a great friend throughout my time here.

- Mohammad ElGamacy for his great efforts and support during my stay in Germany. I would like to thank him for being all the time there to share his opinion and ideas.

- The administrative staff of both IMTEK and the IMBS for the help in all administrative aspects in Germany, namely Frau. Yvonne Weigand, Frau Petra Hettich and Frau Zahra Dandani. I deeply thank all of you for the support.

- My family for their support and for their efforts in making me the person I am today.

- Finally, all the CPI group members for their support and making it easier to pursue science.